An FGF-driven feed-forward circuit for spatiotemporal patterning of the cardiopharyngeal mesoderm in a simple chordate

Florian Razy-Krajka, Basile Gravez and Lionel Christiaen*

Center for Developmental Genetics, Department of Biology, College of Arts and Science, New York University, New York, NY, USA

* author for correspondence: email: lc121@nyu.edu, twitter: @lionlchristiaen, phone: +1 212 992 8695

Abstract

In embryos, pluripotent stem cells and multipotent progenitors must divide and produce distinct progeny to express their full developmental potential. In vertebrates, mounting evidence point to the existence of multipotent cardiopharyngeal progenitors that produce second-heart-field-derived cardiomyocytes, and branchiomeric skeletal head muscles. However, the cellular and molecular mechanisms underlying these early fate choices remain largely elusive. The tunicate *Ciona* has emerged as an attractive model to study early cardiopharyngeal development at high spatial and temporal resolution: through two asymmetric and oriented cell divisions, defined multipotent cardiopharyngeal progenitors produce distinct first and second heart precursors, and pharyngeal muscle (aka atrial siphon muscle, ASM) precursors. Here, we demonstrate that differential FGF/MAPK signaling distinguishes between MAPK-negative heart precursors, and MAPK-positive multipotent progenitors and ASM precursors. We characterize an FGF/MAPK-driven feed-forward circuit that promotes the successive activations of essential cardiopharyngeal determinants, *Tbx1/10* and *Ebf*. Finally, we show that coupling FGF/MAPK restriction and cardiopharyngeal network deployment with cell divisions permits the emergence of diverse cell types from common multipotent progenitors.

Introduction

In the past few years, studies guided by developmental genetics knowledge progressed towards driving mammalian stem cells into forming pure cultures of selected cell types *in vitro* (e.g. (Kattman et al., 2011; Mazzoni et al., 2011; Peljto and Wichterle, 2011). By contrast, in their embryonic context, pluripotent cells generate diverse cell types in defined proportions. This simple observation implies that pluripotent stem cells and multipotent embryonic progenitors must divide before individual cells among their progeny adopt distinct fates, as a result of differential exposure to inducing signals and/or inheritance of cell autonomous determinants.

Subsets of the heart and head/neck myocytes recently emerged as related derivatives of multipotent progenitors located in the mesodermal cardiopharyngeal field (Diogo et al., 2015; Tzahor, 2009; Tzahor and Evans, 2011). Specifically, early lineage tracing, transplantations and controlled explant culture experiments demonstrated that the anterior splanchnic/pharyngeal mesoderm of amniote embryos can produce either skeletal muscles or heart tissue, depending upon exposure to growth factors and signaling molecules (Nathan et al., 2008; Tirosh-Finkel et al., 2006; Tzahor et al., 2003; Tzahor and Lassar, 2001). Clonal analyses in the mouse further revealed the existence of common *Mesp1*-expressing progenitors for subsets of the second heart field-derived cardiomyocytes and branchiomeric facial, jaw, neck and even esophageal muscles (Gopalakrishnan et al., 2015; Lescroart et al., 2014; Lescroart et al., 2015; Lescroart et al., 2010; Lescroart et al., 2012). *In vitro* studies using pluripotent stem cells indicated that controlled *Mesp1* expression can drive mesodermal progenitors towards cardiac and/or skeletal muscle fates (Bondue et al., 2008; Chan et al., 2016; Chan et al., 2013). Genetic labeling and functional studies showed that proper development of the pharyngeal apparatus and second heart field derivatives require shared inputs from Tbx1, Nkx2-5 and Islet1 transcription factors (e.g. (Cai et al., 2003; George et al., 2015;

Jerome and Papaioannou, 2001; Kelly et al., 2004; Merscher et al., 2001; Mosimann et al., 2015; Nevis et al., 2013; Prall et al., 2007; Tzahor and Evans, 2011; Vitelli et al., 2002a; Watanabe et al., 2012; Witzel et al., 2017; Yagi et al., 2003; Zhang et al., 2006)). Taken together, a growing body of evidence point to the existence of a mesodermal field of multipotent progenitors capable of producing either SHF-derived cardiomyocytes or branchiomeric skeletal muscles in early amniote embryos (Diogo et al., 2015; Mandal et al., 2017). However, the mechanisms that distinguish fate-restricted heart and head muscle precursors remain largely elusive.

The tunicate *Ciona*, which is among the closest living relatives to the vertebrates (Delsuc et al., 2006; Putnam et al., 2008), has emerged as a simple chordate model to characterize multipotent cardiopharyngeal progenitors and the mechanisms that initiate heart vs. pharyngeal muscle fate choices (Kaplan et al., 2015; Razy-Krajka et al., 2014; Stolfi et al., 2010; Tolkin and Christiaen, 2016; Wang et al., 2013). *Ciona* tailbud embryos possess two multipotent cardiopharyngeal progenitors on either side. Like their vertebrate counterparts, these cells emerge from *Mesp*+ progenitors towards the end of gastrulation; they are induced by FGF/MAPK signaling and have been termed *trunk ventral cells* (aka TVCs; (Christiaen et al., 2008; Davidson and Levine, 2003; Davidson et al., 2006; Davidson et al., 2005; Satou et al., 2004; Stolfi et al., 2010)). TVCs activate conserved cardiac markers, including *Hand*, *Gata4/5/6* and *Nk4/Nkx2-5*, and migrate as bilateral polarized pairs of cells, until the left and right pairs meet at the ventral midline and begin to divide asymmetrically along the mediolateral axis (Figure 1A; (Christiaen et al., 2008; Davidson et al., 2005; Satou et al., 2004; Stolfi et al., 2010)). The first oriented asymmetric divisions produce small median first heart precursors (FHPs), and large lateral second trunk ventral cells (STVCs), which specifically activate *Tbx1/10* expression (Davidson et al., 2005; Stolfi et al., 2010; Wang et al., 2013). STVCs later divide again to produce small median second heart precursors (SHPs), and large

lateral atrial siphon muscle founder cells (ASMFs), which activate *Ebf* (aka *COE*; (Razy-Krajka et al., 2014; Stolfi et al., 2010; Stolfi et al., 2014c)). The transcription factors Hand-related (Hand-r)/Notrlc, which is expressed in the TVCs and maintained in the STVCs and ASMFs after each division, and Tbx1/10 are required for *Ebf* activation in the ASMFs, whereas Nk4/Nkx2-5 represses *Tbx1/10* and *Ebf* expression in the second heart precursors (SHPs)(Razy-Krajka et al., 2014; Tolkin and Christiaen, 2016; Wang et al., 2013). Conversely, Tbx1/10 and Ebf inhibit cardiac markers, and likely determinants, such as *Gata4/5/6* and *Hand* (Razy-Krajka et al., 2014; Stolfi et al., 2010; Stolfi et al., 2014a; Wang et al., 2013). These regulatory cross-antagonisms presumably underlie the transition from transcriptionally primed multipotent progenitors to separate fate-restricted precursors, by limiting the deployment of the heart- and pharyngeal-muscle-specific programs to their corresponding specific precursors (Kaplan et al., 2015).

Here, we identify regulatory mechanisms ensuring the emergence of diverse fate-restricted precursors from multipotent progenitors. We show that differential FGF/MAPK signaling, feed-forward regulatory mechanisms and coupling with the cell cycle control the spatially restricted activation of *Tbx1/10* and *Ebf*, successively, thus permitting the emergence of both first and second heart precursors, and ASM/pharyngeal muscle precursors from common multipotent progenitors.

Results

MAPK signaling is active in the multipotent cardiopharyngeal progenitors and progressively restricted to the pharyngeal muscle precursors.

During the earliest stages of cardiopharyngeal development in ascidians, multipotent progenitors co-express early regulators of both the heart and ASM programs, a phenomenon referred to as multilineage transcriptional priming, (Razy-Krajka et al., 2014; Stolfi et al., 2014b). Subsequent regulatory cross-antagonisms lead to the segregation of these distinct cardiopharyngeal programs to their corresponding fate-restricted progenitors (Stolfi et al., 2010; Wang et al., 2013); reviewed in (Kaplan et al., 2015)). ASM-specific expression of *Ebf* is necessary and sufficient to terminate the heart program and impose a pharyngeal muscle fate (Razy-Krajka et al., 2014; Stolfi et al., 2010). Antagonistic Tbx1/10 and Nk4 activities determine ASM-specific *Ebf* activation (Wang et al., 2013); however, the symmetry-breaking events leading to cardiopharyngeal mesoderm patterning and ASM-specific expression of *Ebf* remain unknown. In particular, we surmised that differential signaling inputs determine the stereotyped spatio-temporal patterning of early cardiopharyngeal progenitors.

The *Ciona* homologs of specific FGF/MAPK pathway components, including *FGF receptor substrate 2/3* (*Frs2/3*; (Gotoh et al., 2004)*)*, *Ets.b*, and *Fgf4/5/6*, are preferentially expressed in the TVCs, in the STVCs and in the ASMFs as cells transition from a multipotent progenitor state to distinct heart vs. ASM fate-restricted precursors (Razy-Krajka et al., 2014). This patterned expression of MAPK effector genes prompted us to evaluate a role for FGF/MAPK pathway in cardiopharyngeal fate decisions.

We first used an antibody specific to the dual phosphorylated form of Extracellular Regulated Kinase (dpERK) to monitor Mitogen Activated Protein Kinase (MAPK) activity in the cardiopharyngeal mesoderm. We detected dpERK staining in the newly

born TVCs, marked by the B7.5-lineage-specific *Mesp>H2B::mCherry* transgene, as previously observed (Davidson et al, 2006). We also detected weaker but persistent dpERK staining in the TVCs during migration (Figs. 1 and S1). Following the first and second asymmetric divisions of the TVCs and STVCs, dpERK staining was successively restricted to the more lateral STVCs and ASMFs, respectively (Figures 1A, B; S1).

The canonical FGF/Ras/MEK/ERK pathway is necessary and sufficient to promote pharyngeal muscle specification in the cardiopharyngeal lineage.

This exclusion of MAPK activity from the medial first and second heart precursors opened the possibility that differential ERK activity is required for proper STVC and ASMF vs. heart precursors fate decisions. In *Ciona*, signaling through the sole FGF receptor (FGFR) governs ERK activity in several developmental processes, including neural induction (Bertrand et al., 2003; Hudson et al., 2003) and central nervous system patterning (Haupaix et al., 2014; Racioppi et al., 2014; Stolfi et al., 2011; Wagner et al., 2014), early endomesoderm and notochord fate specification (Imai et al., 2002; Picco et al., 2007; Shi and Levine, 2008; Shi et al., 2009; Yasuo and Hudson, 2007). Notably, FGF/MAPK signaling is active in the only *Mesp*+ cardiogenic B7.5 blastomeres (Imai et al., 2006; Shi and Levine, 2008), where targeted misexpression of a dominant negative form of FGFR (dnFGFR) using a B7.5-lineage-specific *Mesp* driver blocks TVC induction (Davidson et al., 2006). We used a TVC-specific *FoxF* enhancer (*FoxF(TVC):bpFOG-1>dnFGFR::mCherry*, hereafter called *FoxF>dnFGFR*; (Beh et al., 2007)), to bypass early effects and achieve later misexpression of dnFGFR in the TVCs and their progeny. *FoxF>dnFGFR* prevented neither TVC migration nor asymmetric divisions, but it abolished the expression of both *Tbx1/10* in the STVCs and *Ebf* in the ASMFs (Figure 1C). This data indicate that FGF/MAPK signaling is required in the cardiopharyngeal

progenitors and/or their progeny for ASM fate specification, beyond the initial TVC induction.

Upon FGF/MAPK-dependent induction, the TVCs express *Hand-related/Hand-r* (renamed after *Notrlc/Hand-like*; (Christiaen et al., 2008; Davidson and Levine, 2003; Davidson et al., 2006; Satou et al., 2004; Stolfi et al., 2014c; Woznica et al., 2012)), which encodes a basic helix-loop-helix (bHLH) transcription factor necessary for *Ebf* expression in the ASMFs (Razy-Krajka et al, 2014). Moreover, the *Hand-r* TVC enhancer contains putative Ets1/2 binding sites, which are necessary for reporter gene expression, and presumably mediate the transcriptional inputs of FGF/MAPK (Woznica et al., 2012). Since *Hand-r* and *FoxF* expressions start at approximately the same time in newborn TVCs, we used *FoxF>dnFGFR* to test whether the maintenance of *Hand-r* expression in migratory TVCs requires prolonged FGF/MAPK inputs after initial TVC induction. *FoxF>dnFGFR* inhibited *Hand*-r expression in late TVCs (Figure 1C), indicating that sustained *Hand-r* expression requires continuous FGF/MAPK signaling.

To test whether the spatial restriction of MAPK activity explains the patterned expressions of *Hand-r*, *Tbx1/10* and *Ebf* following asymmetric cell divisions, we used gain-of-function perturbations to force FGF/MAPK activity throughout the cardiopharyngeal mesoderm and assayed gene expression (Figure 2). We focused on the canonical FGF/MAPK pathway where signal transduction involves Ras, Raf, MEK and ERK downstream of FGFR and upstream of transcriptional effectors (Lemmon and Schlessinger, 2010). We first used M-Ras^{G22V}, a defined constitutively active form of M-Ras, which mediates FGF signaling in *Ciona*, where other classical *Ras* genes are missing (Keduka et al., 2009). To assay the transcriptional consequences of forced M-Ras activity in the cardiopharyngeal lineage, we first focus on *Htr7* and *Tbx1/10* expression following the first asymmetric TVC division in 15 hours post-fertilization (hpf) embryos. *Htr7* encodes a *trans*-membrane G-protein coupled receptor and, like *Hand-r*, its expression

and maintenance in the TVCs require MAPK activity (Figure S2; (Razy-Krajka et al., 2014)), and become restricted to the lateral STVC following asymmetric division. However, *Htr7* mRNAs appear to be cleared more rapidly from the FHPs, making the patterned expression easier to analyze than that of *Hand-r* (Figures 2 and 3D; (Razy-Krajka et al., 2014)). Importantly, misexpression of M-Ras^{G22V} using the TVC-specific *FoxF* enhancer did not alter the cell division patterns, allowing us to identify large lateral STVCs and small median FHPs. Compared to control embryos overexpressing wild-type M-Ras (M-Ras^{WT}), TVC-specific gain of M-Ras function caused both persistent *Htr7* expression and ectopic activation of *Tbx1/10* in the first heart precursors following asymmetric divisions. Similarly, *FoxF>M-Ras^{G22V}*-expressing 18hpf larvae displayed ectopic *Ebf* activation throughout the cardiopharyngeal mesoderm (Figure 2B, C). These results indicated that forced M-Ras activation throughout the cardiopharyngeal lineage is sufficient to ectopically activate STVC and ASMF markers. This is consistent with the idea that spatially defined signaling upstream of M-Ras restricts MAPK activity, thus localizing STVC- and ASM-specific gene activities.

To further probe the signal transduction pathway, we engineered a constitutively active version of the *Ciona* Mek1/2 protein by introducing phosphomimetic mutations of two conserved serine residues in the catalytic domain, as previously shown for the mammalian homolog (Cowley et al., 1994; Mansour et al., 1994). Early misexpression of this Mek^{S220E,S216D} construct in the B7.5 blastomeres using a *Mesp* enhancer caused ectopic TVC induction, mimicking the effects of published gain of Ets1/2 function (Figure S3; (Davidson et al., 2006)). Mirroring the effects of M-Ras^{G22V} gain-of-function experiments, TVC-specific misexpression of Mek^{S220E,S216D} using the *FoxF* enhancer also caused ectopic expression of *Htr7* and *Tbx1/10*, and *Ebf* in 15 and 18hpf larvae, respectively (Figure 2B, C). Taken together, these results indicate that activity of the canonical FGF-Ras-MEK-ERK pathway is progressively restricted to the STVC and

ASMF, and is both necessary and sufficient to promote STVC- and ASMF-specific gene expressions.

Continuous FGF/MAPK activity is required for the successive activations of *Tbx1/10* and *Ebf*.

FGF/MAPK signaling is sufficient and necessary to maintain *Hand-r* expression in late TVCs (Figure 1), and *Hand-r* is necessary for *Ebf* expression in the ASMF (Razy-Krajka et al., 2014). Therefore, it is possible that later FGF/MAPK signaling is dispensable for *Tbx1/10* and *Ebf* activation and ASM specification, as long as STVC and ASMF cells inherit sustained levels of *Hand-r* mRNAs and/or proteins. To disentangle late from early requirements of FGF/MAPK signaling for TVC progeny specification, we incubated embryos at different stages with the MEK/Mapkk inhibitor U0126, which abolishes dual ERK phosphorylation and the initial MAPK-dependent TVC induction in *Ciona* embryos (Figure S1; (Davidson et al., 2006; Hudson et al., 2003)). MEK inhibition during TVC migration (i.e. between 9.5 and 12.5 hpf, Figure 3A) blocked the expression of *Hand-r* and *Htr7* in late TVCs (Figure 3B, E). Similarly, U0126 treatments in late TVCs, and through the first asymmetric division (i.e. between 12 and 15 hpf, Figure 3A) blocked both the maintenance of *Hand-r* and *Htr7*, and the activation of *Tbx1/10* in the STVCs (Figure 3C, D, F, G). Finally, MEK inhibition in late STVCs and through asymmetric divisions (i.e. between 15 and 18 hpf) blocked the ASMF-specific expression of *Ebf* (Figure 3H). These results indicate that continuous MEK activity is required throughout cardiopharyngeal development to successively activate TVC-, STVC-, and ASMF-expressed genes.

Since *Ebf* expression is maintained for several days in the ASMF derivatives as they differentiate into body wall and siphon muscles (Razy-Krajka et al., 2014), we tested whether continued MEK activity is also required for the maintenance of *Ebf* expression

229 past its initial onset and cells' commitment to an ASM fate. Using both regular and
230 intron-specific antisense probes, which specifically detect nascent transcripts (Wang et
231 al., 2013), we showed that later MEK inhibition (i.e. U0126 incubation between 17 and
232 20 hpf) did not block the maintenance of *Ebf* transcription in the ASMPs (Figure 3I, J).
233 This indicates that sustained MEK activity is required until the onset of *Ebf* expression,
234 but not beyond, the maintenance of *Ebf* expression during ASM development is
235 independent of MAPK.
236
237 Since U0126 treatments affect the whole embryo, we sought to further confirm the
238 later roles for FGF/MAPK signaling specifically in the cardiopharyngeal mesoderm. To
239 this aim, we used an STVC-specific enhancer from the *Tbx1/10* locus (termed *T12*; Figure
240 3K, L; (Tolkin and Christiaen, 2016); Racioppi et al., in preparation) to drive expression
241 of either dnFGFR or the constitutively active M-Ras^{G22V} starting at ~14hpf, and assayed
242 *Ebf* expression at 18hpf (Figure 3K, L). These perturbations minimally affected the cell
243 division patterns, such that cells corresponding to FHP, SHP and ASMF could be
244 identified by their position relative to the midline (Figure 3K). M-Ras^{G22V} misexpression
245 caused conspicuous ectopic *Ebf* expression in the SHPs, whereas dnFGFR-mediated
246 inhibition of MAPK activity blocked *Ebf* activation in the lateral ASMFs. These results
247 support the notion that localized FGF/MAPK activity is necessary and sufficient for
248 ASMF-specific expression of *Ebf*.
249
250 **Coherent feed-forward circuits for cardiopharyngeal mesoderm patterning**
251 **and ASM fate specification.**
252 The above results indicate that *Hand-r*, *Tbx1/10* and *Ebf* require ongoing
253 FGF/MAPK activity for their successive activations in the TVCs, STVCs and ASMFs,
254 respectively. We previously showed that RNAi and/or CRISPR-mediated inhibition of

either *Hand-r* or *Tbx1/10* function blocks *Ebf* activation in the ASMFs, where both *Hand-r* and *Tbx1/10* expressions are maintained (Razy-Krajka et al., 2014; Tolkin and Christiaen, 2016; Wang et al., 2013). Therefore, observations such as the loss of *Ebf* expression upon *FoxF>dnFGFR* electroporation could be due to an early loss of *Hand-r* and/or *Tbx1/10*. We used epistasis assays to systematically test whether early regulators mediate the effects of FGF/MAPK on later gene expression and ASM fate specification, or whether FGF/MAPK signaling acts both upstream and in parallel to early regulators in a more complex regulatory circuit.

We first revisited the regulatory relationships between FGF/MAPK, *Hand-r* and *Tbx1/10* in late TVCs and early STVCs. We validated single guide RNAs (sgRNAs) for CRISPR/Cas9-mediated mutagenesis of *Hand-r* (Table S1; (Gandhi et al., 2017)), and determined that *Hand-r* function is necessary for *Tbx1/10* activation in the STVCs (Figure 4A). Co-expression of a modified *Hand-r* cDNA containing wobble base mutations that disrupt the sgRNA protospacer adjacent motif (PAM; Hand-r^{PAMmis}) rescued *Tbx1/10* expression in the STVCs, indicating that *Tbx1/10* down-regulation in this CRISPR "background" is specifically due to *Hand-r* loss-of-function (Figure 4A). To further probe if *Hand-r* activity is necessary for FGF/MAPK-dependent *Tbx1/10* expression, we used gain of M-Ras function in a *Hand-r* CRISPR "background". Whereas, misexpression of the constitutively active M-Ras^{G22V} caused ectopic *Tbx1/10* expression, concomitant loss of *Hand-r* function diminished both endogenous and ectopic *Tbx1/10* expression in the STVC and FHP, respectively (Figure 4A). Although, remaining ectopic activation could still be observed, possibly because M-Ras^{G22V} could boost *Hand-r* expression in heterozygous cells where CRISPR/Cas9 disrupted only one copy of the gene. This data indicate that *Hand-r* is necessary for FGF/MAPK-induced activation of *Tbx1/10*.

To further probe the epistatic relationships between *Hand-r* and MAPK signaling upstream of *Tbx1/10*, we attempted to rescue *Tbx1/10* expression in U0126-treated embryos, by over-expressing *Hand-r* with the TVC-specific *FoxF* enhancer. Neither did Hand-r over-expression cause ectopic *Tbx1/10* activation (in the FHPs), nor was it sufficient to rescue *Tbx1/10* expression in 15hpf STVCs (Figure 4B). Taken together, these data indicate that both Hand-r and MAPK activities are required to activate *Tbx1/10* in the STVCs. These results also imply that MAPK signaling is restricted to the STVC independently of Hand-r activity, which suffice to explain the STVC-specific activation of *Tbx1/10*.

Next, we investigated the epistatic relationship between FGF/MAPK, *Hand-r*, and *Tbx1/10* upstream of *Ebf* in the ASMFs. We first used previously validated CRIPSR/Cas9 reagents targeting the *Tbx1/10* coding region (Tolkin and Christiaen, 2016), to confirm that B7.5-lineage-specific loss of *Tbx1/10* function inhibited *Ebf* activation, and verified that this effect could be rescued by over-expression of a CRISPR/Cas9-resistant *Tbx1/10* cDNA, expressed with a minimal TVC-specific *FoxF* enhancer (Figure 4C; Tbx1/10^{PAMmis}). In these rescue experiments, we observed ectopic *Ebf* activation in the SHP, as previously described when driving Tbx1/10 expression with a TVC-specific *FoxF* enhancer (Wang et al., 2013). As explained below, this ectopic activation could be attributed to a precocious expression of *Ebf* in the STVCs (Figure 4E). To test whether *Tbx1/10* was also required for ectopic *Ebf* expression in response to MAPK activation, we combined CRISPR/Cas9-mediated *Tbx1/10* knockout with constitutive MAPK activation using the M-Ras^{G22V} mutant and observed a significant inhibition of both endogenous and ectopic *Ebf* expression in the 18hpf ASMF and SHP, respectively (Figure 4C). Taken together, these results show that *Tbx1/10* function is necessary for FGF/MAPK-induced expression of *Ebf* in the ASMFs.

306 To further test whether *Tbx1/10* acts in parallel and/or downstream of MAPK to
307 activate *Ebf*, we combined gain of *Tbx1/10* function with perturbations of FGF/MAPK
308 signaling and assayed *Ebf* expression. We realized that *FoxF*-driven misexpression of
309 Tbx1/10 caused precocious *Ebf* activation in 15hpf STVCs (Figure 4D, E). This precocious
310 expression remained remarkably patterned, suggesting that STVC-restricted FGF/MAPK
311 activity prevented *Ebf* expression in the dpERK-negative, small median FHPs (Figures
312 1B, 4E, S1). Indeed, co-expression of both Tbx1/10 and M-Ras^{G22V} caused both
313 precocious and ectopic *Ebf* expression in the 15hpf medial and lateral TVC derivatives,
314 which would be FHPs and STVCs in control embryos, respectively. This data confirms
315 that Tbx1/10 misexpression does not suffice to cause ectopic *Ebf* expression in the FHPs,
316 because the latter presumably lack FGF/MAPK activity, as is the case in control embryos.
317 U0126-mediated MEK inhibition from 12 to 15hpf, i.e. after the onset of
318 *FoxF>Tbx1/10* misexpression, further confirmed that MAPK activity is required in
319 parallel to Tbx1/10 for precocious *Ebf* activation in 15hpf STVCs (Figure 4D, E). Taken
320 together, these results indicate that Tbx1/10 and MAPK are both required to activate *Ebf*
321 in the cell cycle following that of *Tbx1/10* onset.
322
323 Since *Hand-r* expression is maintained in the ASMF, and CRISPR/Cas9- or RNAi-
324 mediated *Hand-r* knockdown blocked both *Tbx1/10* (Figure 4A) and *Ebf* expression
325 (Razy-Krajka et al., 2014), we reasoned that Hand-r could also act both upstream and in
326 parallel to Tbx1/10 for *Ebf* activation. To test this possibility, we assayed *Ebf* expression
327 in 18hpf ASMF following defined perturbations of Hand-r and Tbx1/10. As expected,
328 CRISPR/Cas9-mediated *Hand-r* mutagenesis strongly inhibited *Ebf* expression, and this
329 effect could be rescued by a CRISPR-resistant *Hand-r* cDNA (Figure 4F). To test
330 whether this effect was mediated by a loss of *Tbx1/10* expression, we attempted to rescue
331 the Hand-r loss-of-function by over-expressing Tbx1/10 using the *FoxF* enhancer. As

explained above, *FoxF*-mediated Tbx1/10 misexpression caused precocious and ectopic *Ebf* expression in larvae co-electroporated with control sgRNAs (Figure 4D, E, F). By contrast, combining loss of Hand-r function with Tbx1/10 misexpression inhibited both the endogenous and ectopic *Ebf* expression (Figure 4F), indicating that Hand-r is also required in parallel to Tbx1/10 for *Ebf* activation in the ASMFs.

Taken together, these analyses of the epistatic relationships between FGF/MAPK signaling, *Hand-r*, *Tbx1/10* and *Ebf* suggest that coherent feed-forward circuits govern the sequential activation of *Hand-r*, *Tbx1/10* and *Ebf* in response to continuous but progressively restricted FGF/MAPK inputs (Figure 4G), thus linking spatial patterning to the temporal deployment of the regulatory cascade leading to localized *Ebf* activation and pharyngeal muscle specification.

The cell cycle entrains the temporal deployment of the cardiopharyngeal gene regulatory network.

In principle, the feed-forward circuit described above is sufficient to explain the successive activations of *Hand-r*, *Tbx1/10* and *Ebf*. However, *Tbx1/10* and *Ebf* do not turn on until after oriented and asymmetrical divisions of the TVCs and STVCs, respectively. Notably, even when we misexpressed Tbx1/10 in the TVCs, *Ebf* was activated only after TVC division and in the lateral-most cells, where FGF/MAPK signaling is normally maintained (Figures 1B, 4E). This sequence of events -divisions followed by gene activation- is paramount in the cardiopharyngeal mesoderm, as it permits the birth of first and second heart precursors, whose fates are antagonized by Tbx1/10 and Ebf (Razy-Krajka et al., 2014; Stolfi et al., 2010; Wang et al., 2013). Therefore, we sought to investigate the role(s) of the cell cycle in controlling the timing of *Tbx1/10* and *Ebf* activations.

We first evaluated the effects of cytochalasin B, a classic inhibitor of cytokinesis widely used to study cell fate specification in ascidians (Figure 5A; (Whittaker, 1973)). Treatments starting before TVC divisions (12 hpf) did not block *Tbx1/10* or *Ebf* expression in embryos fixed after their normal onset at either 16 or 19hpf, respectively (Figure 5B). Similarly, treatment starting between the first and second asymmetric divisions (15hpf) did not block localized *Ebf* expression at 19hpf (Figure 5B). This indicates that *Tbx1/10* and *Ebf* activations occur by default in the absence of cytokinesis, most likely because FGF/MAPK signaling persists throughout the shared cytoplasm. This data thus illustrates how the spatial restriction of FGF/MAPK signaling, following cell divisions, leads to the localized activations of *Tbx1/10* and *Ebf*, and permits the emergence of first and second cardiac precursors.

Cytochalasin treatments usually lead to the formation of polynucleated cells (e.g. Figure 5B, middle panel), because the cell cycle and nucleokinesis continue in these artificial endoreplicating cells. To alter cell cycle progression more comprehensively, and specifically in the cardiopharyngeal lineage, we used genetically encoded inhibitors of cell cycle transitions: Cdkn1b.a and Cdkn1b.b (also known as Noto16), the ortholog of which is a potent inhibitor of the G1/S transition in the ascidian species *Halocynthia roretzi* (Kuwajima et al., 2014), and Wee1, a G2/M inhibitor, as previously described (Dumollard et al., 2017). We used the TVC-specific *FoxF* enhancer to misexpress these negative regulators of cell cycle progression, monitored cell divisions and assayed *Tbx1/10* expression at 15hpf, when control TVCs have divided and the lateral-most STVCs normally express *Tbx1/10*. Each perturbation efficiently inhibited TVC divisions, such that only two cells were visible on either side of the embryos (Figure 5C). In these delayed TVCs, *Tbx1/10* expression was strongly reduced compared to control STVCs (Figure 5C; compare to Figure 4A, B). However, approximately 40% of the delayed TVCs expressed *Tbx1/10* to variable extents. This suggests that the cardiopharyngeal

383 regulatory network can qualitatively unfold independently of cell cycle progression, but
384 the latter is necessary for *Tbx1/10* expression to its wild-type levels.

385 We next used the STVC-specific *Tbx1/10 T12* enhancer, to misexpress Cdkn1b.a,
386 Noto16 and Wee1, and assay *Ebf* expression at later stages. Inhibitors of the G1/S
387 transition failed to block STVC divisions (data not shown), most likely because *T12*-
388 driven products did not accumulate quickly enough to interfere with the G1/S transition
389 in STVCs (this cell cycle lasts only ~2 hours compared to ~6 hours for the TVC
390 interphase), suggesting that the G1 phase is too short for *T12*-driven gene products to
391 accumulate before the G1/S transition. Therefore, we focused the analyses of *Ebf*
392 response to cell cycle perturbations on misexpression of the G2/M inhibitor Wee1.
393 Preliminary analyses of 18hpf larvae, fixed approximately 2 hours after the documented
394 onset of *Ebf* expression in ASMFs (Razy-Krajka et al., 2014), indicated that *Ebf* can turn
395 on in arrested STVCs that failed to divide upon Wee1 misexpression (Figure 5D).

396 Because ~30% of the embryos showed variable expression, as was the case for
397 *Tbx1/10* in the previous experiment, we reasoned that perturbations of the G2/M
398 transition could alter the dynamics of *Ebf* upregulation. We investigated this possibility
399 using embryos fixed every 30 minutes between 15.5hpf and 18hpf, when cells transition
400 from a late *Tbx1/10*+; *Ebf*- STVC state to a committed *Ebf*+, *Mrf*+ ASMF state (Razy-
401 Krajka et al., 2014; Wang et al., 2013). First, we observed that the proportion of embryos
402 with conspicuous ASMFs increased from ~20% to >90% between 15.5 and 16.5 hpf in
403 control embryos (Figure 4E). By contrast, Wee1-expressing cells had divided in only
404 ~35% of the embryos by 16.5hpf, and that proportion gradually increased to ~70% by
405 18hpf (Figure 4E), indicating that Wee1 misexpression strongly delays cell cycle
406 progression, blocking cell divisions in a substantial fraction of embryos.

407 Focusing on ASMFs, we found that the proportion of *Ebf*+ cells in control embryos
408 progressively increased from ~20% showing "weak" expression at 15.5hpf to >90%

showing "strong" expression by 18hpf (Figure 5F; see Figure 5D for examples of "weak" and "strong" expression). This semi-quantitative analysis revealed an under-appreciated dynamic at the onset of *Ebf* expression, which appears to take at least one hour to be "strongly" expressed in >75% of newborn ASMFs (Figure 4F).

To evaluate the impact of Wee1-induced mitosis inhibition on *Ebf* accumulation, we focused on undivided STVCs at each time point (hence the lower numbers in Figure 4F compare to Figure 4E). By 17hpf, wee1-expressing delayed STVCs showed "strong" *Ebf* expression in comparably high proportions of embryos. However, these proportions were significantly lower at 16 and 16.5hpf (Chi-square tests, P=0.002 and P=0.0003, respectively), with ~1.5 and ~1.2 times less "strongly" expressing cells than in the control distributions (hypergeometric tests, P=0.0005 and P=0.0001, respectively). These semi-quantitative data suggests that the cardiopharyngeal network can eventually unfold and lead to high levels of *Ebf* expression independently of cell divisions, albeit with a delay revealing that cell divisions probably entrain *Ebf* upregulation in early ASMFs.

Transition from a MAPK-dependent to a MAPK-independent and autoregulative mode of *Ebf* expression in early ASMFs.

Given the semi-quantitative nature of our analysis, and the relatively subtle effects observed on *Ebf* dynamics, we sought to further probe the mechanisms that regulate the onset and upregulation of *Ebf* expression in early ASMFs, and the biological significance for cell-fate specification. Since we observed a progressive accumulation of *Ebf* mRNAs, and a transition from a MAPK-dependent onset to a MAPK-independent maintenance of *Ebf* transcription (Figure 3I, J), we reasoned that the window of MAPK-dependence might coincide with the accumulation of *Ebf* mRNAs between 16 and 17hpf. To test this possibility, we treated embryos with the MEK inhibitor U0126 at successive time points, assayed ongoing transcription using intronic probes and counted the numbers of *Ebf*

435 transcribing cells (Figure 6A). This analysis revealed that *Ebf* transcription gradually lost
436 its sensitivity to MAPK inhibition between 16 and 17hpf, i.e. during the first hour of the
437 ASMF cycle when *Ebf* mRNAs normally accumulate (as shown in Figure 5E, F).

438 Because *Ebf* transcription becomes independent from MAPK by the time *Ebf* mRNA
439 have accumulated to "high" levels, and because *Ebf* expression lasts for several days in
440 the progeny of the ASMFs, we reasoned that autoregulation might suffice to maintain
441 high levels of *Ebf* mRNA past the MAPK-dependent onset. To test this possibility, we
442 misexpressed the Ebf coding sequence using the STVC-specific *T12* enhancer as
443 described (Tolkin and Christiaen, 2016). Assaying endogenous *Ebf* transcription using
444 intronic probes demonstrated that, in addition to its normal expression in the ASMFs,
445 Ebf misexpression caused precocious and ectopic activation of the endogenous locus in
446 the STVCs, and in the MAPK-negative SHPs, respectively (Figure 6C-F). This result
447 suggests that *Ebf* transcription bypasses both requirements for cell-division coupling and
448 MAPK inputs if high levels of *Ebf* gene products are present in the cell.

449 We reasoned that, if high levels of *Ebf* expression can promote its own transcription
450 independently of MAPK signaling, then Ebf misexpression should be sufficient to rescue
451 a chemical inhibition of MAPK at a critical stage. We tested this possibility by combining
452 Ebf misexpression using the STVC-specific *T12* enhancer and U0126 treatments starting
453 at 16hpf, which normally block *Ebf* expression (Figure 6A, D-F). We observed that
454 transcription of the endogenous *Ebf* locus became independent of early MAPK activity
455 upon misexpression of an Ebf cDNA, further supporting the notion that high levels of
456 *Ebf* expression suffice to maintain *Ebf* transcription independently of MAPK activity.
457
458 A potentially important implication of this transient MAPK-dependence of is to
459 render *Ebf* expression initially reversible. For instance, *Ebf* occasionally turns on
460 precociously in the STVCs of a small proportion of embryos (Figure S4). Given the

powerful anti-cardiogenic effects of Ebf (Razy-Krajka et al., 2014; Stolfi et al., 2010), persistent *Ebf* expression would have dramatic consequences for SHP development (Wang et al., 2013). However, because MAPK activity is excluded from the SHPs, and the early phase of *Ebf* expression depends upon continuous MAPK activity, we surmise that *Ebf* cannot be maintained in the SHPs. For instance, when embryos from the same electroporated batch were fixed at the time of early U0126 treatment (i.e. 15.75 and 16.25hpf) and ~4 hours later, at 20hpf, and assayed for *Ebf* transcription using intronic probes, initially wild-type patterns of *Ebf* transcription could not be maintained (Figure S5A). This suggests that, although *Ebf* can be activated precociously in a MAPK-dependent manner, its expression shuts off in the SHPs upon MAPK inhibition following STVC division.

We further addressed the interplay between cell division, MAPK signaling and *Ebf* expression. We reasoned that, if cell divisions entrain Ebf accumulation and the transition to a MAPK-independent autoregulative mode, then delaying STVC divisions should extend the period of MAPK-dependent *Ebf* transcription. We tested this possibility by expressing Wee1 under the control of the STVC-specific *T12* enhancer, and treated embryos with U0126 at 17hpf, which inhibited the maintenance of *Ebf* transcription in only 15% to 20% of the control embryos (Figures 6A, S5B). The proportion of embryos showing U0126-sensitive *Ebf* transcription increased to almost 50% upon *T12>Wee1* expression (Figure S5B), which is consistent with our hypothesis that inhibiting the G2/M transition delayed the accumulation of *Ebf* gene products thus postponing the transition from a low level/MAPK-dependent to an high level/MAPK-independent and self-activating mode of *Ebf* regulation.

Taken together these data lead us to propose a model for *Ebf* regulation whereby Hand-r, Tbx1/10, ongoing MAPK signaling and cell-cycle-regulated transcriptional input(s) govern the onset and initial accumulation of *Ebf* gene products during the first

487 hour of the ASMF cycle, whereas the maintenance of *Ebf* expression relies primarily on

488 MAPK-independent autoactivation, following initial accumulation (Figure 7).

Discussion

Here, we demonstrated that the progressive restriction of FGF/MAPK signaling follows asymmetric cell divisions of multipotent progenitors and patterns the ascidian cardiopharyngeal mesoderm in space and time. This leads to the localized expression of *Hand-r*, *Tbx1/10* and *Ebf* in fate-restricted pharyngeal muscle precursors, and their concomitant exclusion for first and second heart precursors. We show that coherent feedforward circuits encode the successive activations of *Hand-r*, *Tbx1/10* and *Ebf*, whereas cell divisions entrain the progression of this regulatory sequence and thus define the timing of gene expression. Finally, we provide evidence that the initiation of *Ebf* expression depends on MAPK activity in early ASMF, until Ebf accumulation permits MAPK-independent auto-activation. Given the potent anti-cardiogenic, and pro-pharyngeal muscle effects of Ebf (Razy-Krajka et al., 2014; Stolfi et al., 2010), we surmise that the latter switch corresponds to the transition from a cardiopharyngeal multipotent state to a committed pharyngeal muscle identity.

Spatial patterning by localized maintenance of FGF/MAPK signaling.

Our results demonstrate that MAPK signaling is maintained only in the lateral-most daughter cells following each asymmetric division of multipotent cardiopharyngeal progenitors - the TVCs and STVCs. This asymmetric maintenance is necessary and sufficient for the progressive and localized deployment of the pharyngeal muscle network. Notably, the TVCs themselves are initially induced by similar polarized FGF/MAPK signaling coincidental to asymmetric cell divisions of their mother cells, aka the B8.9 and B8.10 founder cells (Davidson et al., 2006). Detailed analyses have since indicated that asymmetrical maintenance of sustained FGF/MAPK signaling involves intrinsic Cdc42-dependent polarity of the founder cells, which promotes polarized cell-matrix adhesion of the prospective TVC membrane to the ventral epidermis. The latter

differential integrin-mediated adhesion promotes localized MAPK activation, leading to TVC induction (Cooley et al., 2011; Norton et al., 2013). It has been proposed that adhesion- and caveolin-dependent polarized FGFR recycling during mitosis accounts for the localized activation of MAPK in the prospective TVCs (Cota and Davidson, 2015). Whereas similar mechanisms could in principle account for asymmetric maintenance of FGF/MAPK signaling in STVCs and ASMFs, this has not been formally tested and there are notable differences opening the possibility that other mechanisms may be at work: during TVC induction, MAPK signaling is maintained in the smaller daughter cell that contacts the epidermis, whereas in the following divisions, MAPK activity persists in the larger daughter cells and all cells maintain contact with the epidermis (Nicole Kaplan and Lionel Christiaen, data not shown). Moreover, using an FGFR::mKate2 fusion protein similar to that used in previous studies, we could not observed a marked polarized distribution of FGFR molecules to the lateral-most cells (the STVCs and ASMFs; Yelena Bernadskaya and Lionel Christiaen, data not shown). However, the fact that constitutively active forms of M-Ras and Mek1/2 were sufficient to bypass the loss of MAPK activity, and impose pharyngeal muscle specification, indicates that differential FGF/MAPK activity is regulated upstream of M-Ras. Further work is needed to elucidate the cellular and molecular mechanisms governing the spatiotemporal patterns of FGF/MAPK signaling in the cardiopharyngeal mesoderm. In particular, it will be important to disentangle the relative impacts of extrinsic (i.e. tissues, contacts) vs. intrinsic (i.e. asymmetric cell division) effects onto FGF/MAPK signaling and the downstream transcriptional inputs.

Transcriptional effects of differential FGF/MAPK signaling.

Because differential FGF/MAPK signaling rapidly impacts cell-specific gene expression, we surmise that transcriptional effectors are dynamically regulated. For

instance, even though we have not formally identified the downstream DNA-binding transcription factor (see discussion below), it would be conceivable that the phosphorylated forms of either transcriptional effector persist through cell division upon maintenance of FGF/MAPK activity. However, we have shown that continuous MAPK activity is needed following each division. Therefore, we must invoke elusive phosphatase activities, such as dual-specificity phosphatases (DUSPs; (Patterson et al., 2009), which would reset transcriptional effectors to a dephosphorylated state, thus rendering steady-state FGF/Ras/MAPK inputs necessary.

Systematic dephosphorylation of FGF/MAPK transcriptional effectors is likely to be particularly important for heart fate specification. For instance, whole genome analyses indicate that heart-specific *de novo* gene expression requires MAPK inhibition (Wang et al., 2017). Although the molecular mechanisms remain elusive, one simple possibility is that, lest fate-restricted heart precursors inhibit MAPK activity, they will activate *Tbx1/10* and *Ebf*, which will block the cardiac program (Razy-Krajka et al., 2014; Stolfi et al., 2010; Wang et al., 2013). Finally, we previously proposed that repressor inputs from Nk4 are needed in the second heart precursors to avoid ectopic activation of *Ebf* (Wang et al., 2013). The observation that Nk4 transcripts are detected in all cardiopharyngeal cells opened the question as to how *Ebf* would escape repression by Nk4 in the ASMFs. Differential MAPK activity offers an intriguing possibility: for instance, Nk4/Nkx2-5-mediated repression in other species involves the co-repressor Groucho/TLE (Choi et al., 1999), which is strongly expressed in the cardiopharyngeal mesoderm (Razy-Krajka et al., 2014); and, in flies, MAPK-mediated phosphorylation of Groucho inhibits its repressor function (Cinnamon et al., 2008; Cinnamon and Paroush, 2008; Hasson et al., 2005). Therefore, it is possible that persistent MAPK signaling dampens Groucho/TLE-mediated repressive inputs on cell-specific regulatory genes like *Ebf*. Future studies will

566 determine whether such mechanisms provide bistable switches underlying MAPK-
567 dependent fate choices in the cardiopharyngeal mesoderm.
568
569 **Temporal deployment of the pharyngeal muscle network**
570 The localized and successive activation of *Tbx1/10* and *Ebf* in STVCs, and ASMFs,
571 respectively, are important features of the cardiopharyngeal network that permit the
572 emergence of diverse cell fates: first and second heart precursors, and atrial siphon
573 muscle precursors. Experimental misexpression of Ebf throughout the cardiopharyngeal
574 mesoderm suffice to inhibit heart development (Razy-Krajka et al., 2014; Stolfi et al.,
575 2010), illustrating how important it is for *Ebf* expression to be restricted to the ASMF,
576 once the first and second heart precursors are born and have terminated MAPK activity.
577 Our analyses indicate that the sequential activations of *Hand-r*, *Tbx1/10* and *Ebf* is
578 encoded in the feed-forward structure of this sub-circuit, whereas the continuous
579 requirement for MAPK inputs and their progressive exclusion from heart progenitors
580 restrict the competence to activate *Tbx1/10* and *Ebf* to the most lateral cells, after each
581 division. Our model implies that each gene may directly respond to transcriptional
582 inputs from MAPK signaling. We have not formally identified the transcription factors(s)
583 that mediate the transcriptional response to FGF/MAPK signaling. However,
584 multipotent cardiopharyngeal progenitors express *Ets1/2* and *Elk*, two common
585 transcriptional effectors of FGF/MAPK signaling in *Ciona* (Bertrand et al., 2003;
586 Christiaen et al., 2008; Davidson et al., 2006; Gainous et al., 2015). Moreover, Ets1/2
587 has been implicated in the initial FGF/MAPK-dependent induction of multipotent TVCs
588 (Christiaen et al., 2008; Davidson et al., 2006), and it expression is also progressively
589 restricted to the lateral-most progenitors following each division (Razy-Krajka et al.,
590 2014). Taken together, Ets1/2 and, to some extend, Elk are intriguing candidate
591 transcriptional effectors of FGF/MAPK signaling in cardiopharyngeal development.

592 The binding preferences of Ets-family factors have been extensively studied in *Ciona*,
593 and they do not depart markedly from conserved Ets-family binding sites with a GGAW
594 core (Bertrand et al., 2003; Farley et al., 2015; Farley et al., 2016; Gueroult-Bellone et al.,
595 2017; Khoueiry et al., 2010). Putative Ets-family binding sites in the TVC-specific *Hand-*
596 *r* enhancer are conserved between *Ciona intestinalis* and its sibling species *C. robusta*
597 and *C. savignyi*, and necessary for its activity in reporter assays (Woznica et al., 2012).
598 Similarly, minimal STVC and ASM enhancers for *Tbx1/10* and *Ebf*, respectively, contain
599 conserved putative Ets-family binding sites, although their function has not been tested
600 ((Razy-Krajka et al., 2014; Wang et al., 2013) and data not shown). Taken together, these
601 observations suggest that the proposed feed-forward sub-circuit involves direct
602 transcriptional inputs from FGF/MAPK-regulated Ets-family factors on the
603 cardiopharyngeal enhancers of *Hand-r*, *Tbx1/10* and *Ebf*.
604
605 Whereas the regulatory architecture of the MAPK; Hand-r; Tbx1/10; Ebf sub-circuit
606 explains the sequence of activation events, it is also crucial for its correct deployment,
607 and the generation of diverse cell identities, that genes are not fully activated before
608 successive cell divisions. While divisions are not absolutely required for *Ebf* to eventually
609 turn on, cell cycle progression appears to entrain the deployment of this network,
610 especially for *Tbx1/10* and *Ebf* activation in STVCs and ASMFs, respectively. These
611 observations imply that, while the network can eventually unfold, its intrinsic dynamic is
612 slower than observed. This allows first and second heart precursors to be born prior to
613 the onset of *Tbx1/10* and *Ebf*, respectively. The latter sequence is essentially for the heart
614 progenitors to escape the anti-cardiogenic effects of Tbx1/10 (Wang et al., 2013), and Ebf
615 (Razy-Krajka et al., 2014).
616 Initial *Ebf* expression in early ASMFs is also labile and MAPK-dependent for
617 approximately one hour. This continued requirement for MAPK inputs ensures that, in

the rare instances when *Ebf* expression starts in the multipotent STVC progenitors and/or expands to the nascent SHPs, inhibition of MAPK shuts off *Ebf* expression before it reaches the levels needed for commitment to an ASM fate. Indeed, our results indicate that, once *Ebf* mRNAs have accumulated to high levels, its expression becomes auto-regulative and MAPK-independent. We surmise that this transition coincides with a fundamental switch from a multipotent cardiopharyngeal state to a committed pharyngeal muscle identity.

From this standpoint, the observed entrainment of *Ebf* expression by the cell cycle can be seen as acceleration of the transition to commitment following asymmetric division of multipotent progenitors. Although the mechanisms remain elusive, it is likely that this requires the M/G1 transition, as the G1 phase has been shown to be particularly conducive to the expression of fate-specific regulators in mammalian pluripotent stem cells (Dalton, 2015; Pauklin et al., 2016; Pauklin and Vallier, 2013; Soufi and Dalton, 2016).

Conserved dual effects of FGF/MAPK signaling on heart development in chordates

Previous studies highlighted how FGF/MAPK signaling is necessary along side Mesp during early cardiac development in *Ciona* (Christiaen et al., 2008; Davidson, 2007; Davidson et al., 2006), and how this early requirement also exists in vertebrates (Abu-Issa et al., 2002; Alsan and Schultheiss, 2002; Barron et al., 2000; Brand, 2003; Reifers et al., 2000; Zaffran and Frasch, 2002). We now know that these early FGF/MAPK inputs induce and maintain multipotent cardiopharyngeal states in *Ciona*, including the *Tbx1/10+* multipotent progenitors that eventually produce the second heart lineage ((Razy-Krajka et al., 2014; Stolfi et al., 2010; Wang et al., 2013; Wang et al., 2017), and this study). Similarly, in vertebrates, regulatory interplay between Fgf8 and Fgf10

644 signaling and Tbx1 is required for development of both pharyngeal arch and second
645 heart field derivatives, presumably in part by maintaining an undifferentiated and
646 proliferative state (Abu-Issa et al., 2002; Aggarwal et al., 2006; Brown et al., 2004; Chen
647 et al., 2009; Hu et al., 2004; Ilagan et al., 2006; Kelly and Papaioannou, 2007; Park et
648 al., 2006; Park et al., 2008; Vitelli et al., 2002b; Watanabe et al., 2010; Watanabe et al.,
649 2012). Notably, FGF signaling acts in successive phases, and its inhibition is necessary
650 for final myocardial specification and differentiation (Hutson et al., 2010; Marques et al.,
651 2008; Tirosh-Finkel et al., 2010; van Wijk et al., 2009). Conversely, continued FGF
652 signaling beyond the multipotent mesodermal progenitor stages was shown to promote
653 smooth muscle and epicardial differential in the heart (Hutson et al., 2010; van Wijk et
654 al., 2009), and also myoblast specification and/or skeletal muscle differentiation in the
655 head, with the expression of FGF ligands being maintained in the pharyngeal arches
656 (Bothe et al., 2011; Buckingham and Vincent, 2009; Michailovici et al., 2015;
657 Michailovici et al., 2014; von Scheven et al., 2006). Taken together, these and our data
658 suggest that FGF/MAPK signaling plays evolutionary conserved roles during chordate
659 cardiopharyngeal development, by promoting the specification of successive mesodermal
660 and *Tbx1*+ multipotent states, and a fate-restricted non-cardiac muscle identity, while
661 MAPK inhibition is required for myocardial specification and differentiation in the first
662 and second heart field, successively.

Material and methods

Animals, electroporations, and chemical treatments

Gravid wild *Ciona intestinalis* type A, now called *Ciona robusta* (Pennati et al., 2015), were obtained M-REP (Carlsbad, CA, USA), and kept under constant light to avoid spawning. Gametes from several animals were collected separately for *in vitro* cross-fertilization followed by dechorionation and electroporation as previously described (Christiaen et al., 2009a, b). Different quantities of plasmids were electroporated depending on the constructs. Typically, 50 µg of DNA was electroporated for NLS::lacZ or plain mCherry driving constructs but only 15 µg for *Mesp-1>H2B::mCherry*. For perturbation constructs, 70 µg were usually electroporated, except for *Mesp>NLS::Cas9::NLS* (30 µg) and pairs of U6>sgRNA plasmids (25 µg each). U0126 (Cell Signaling Technology, Danvers, MA) was used at 5µM in artificial seawater from a stock solution of 20mM in DMSO. Cytochalasin B (Sigma, Saint Louis, MO) was used at ~3 µg/mL from a 10 mg/mL stock solution in DMSO as previously performed (Jeffery et al., 2008). Control embryos were incubated in parallel with corresponding concentrations of DMSO alone.

In situ hybridization

In situ hybridizations were carried out essentially as described previously (Christiaen et al., 2009c; Razy-Krajka et al., 2014), using DIG labeled riboprobes, anti-DIG-POD Fab fragments (Roche, Indianapolis, IN), and Tyramide Amplification Signal coupled to Fluorescein (Perkin Elmer, MA). Reporters expressed in the lineage of interest were marked using anti-ß-galactosidase monoclonal mouse antibody (1:1000; Promega, Fitchburg, WI) or anti-mCherry rabbit polyclonal antibody (1:500; BioVision 5993-100), respectively targeted with anti-mouse or anti-rabbit secondary antibody coupled with

Alexa 648 (1:500; Invitrogen, Carlsbad, CA). The different probes used in this study were described previously (Razy-Krajka et al., 2014; Stolfi et al., 2010; Wang et al., 2013).

dpERK/mcherry double fluorescent immunostaining

Samples were fixed, as for *in situ* hybridizations, in MEM-PFA with Tween 20 (0.05%) but only for 30 minutes at room temperature, washed three times in PBSt (Tween 20 0.01%) for 10 minutes, gradually dehydrated every 10 minutes in Ethanol/PBS series (33%, 50%, 80%) and Methanol 100%. Samples were then gradually rehydrated every 10 minutes in Methanol/PBSt series, rinsed three times in PBSt, permeabilized with PBS Triton-100 (0.2%) for 30 minutes and incubated for 2 hours at room temperature with anti-dpERK mouse monoclonal antibody (1:200; Sigma, Saint Louis, MO) and anti-mCherry polyclonal antibody from rabbit (1:500; Biovision, Milpitas, CA) in PBS 0.01% Triton-100 (T-Pbs) supplemented with 2% normal goat serum. Samples were then washed three times in T-PBS and incubated in anti-mouse and anti-rabbit antibodies (1 :500 each), respectively coupled with Alexa 488 and Alexa 568 (Invitrogen, Carlsbad, CA), overnight at 4°C or for 2 hours at room temperature. Finally, samples were rinsed three times in T-PBS for 15 minutes and mounted in Prolong Gold (Molecular Probes, Eugene, OR).

Molecular cloning

Coding sequences for wild-type M-Ras (KH.L172.2), Mek1/2 (KH.L147.22), Cdkn1b.a (Cdkn1b, KH.C14.564), and Cdkn1b.b (Noto16, KH.S643.6) were PCR-amplified from cDNA libraries prepared by reverse transcription of total RNA from mixed developmental stages. Insertion of the products into expressing vectors was performed using regular restriction/ligation or In-fusion (Clontech, Mountain View, CA) procedure. Oligonucleotide directed mutagenesis or two-step overlap PCRs were used to generate

the point mutated forms M-Ras^{G22V} and Mek^{S220E,S216D} from the corresponding wild-type sequences. We also used oligonucleotide directed mutagenesis to generate mismatches in the PAM sequences adjacent to the sgRNA targets for Hand-r (153C>T 574C>T for Hand-r^{PAMmis}) and Tbx1/10 (325G>A and 579G>A for Tbx1/10^{PAMmis}). Due to the absence of a correct PAM sequence (NGG, (reverse complement CCN)), overexpressed Hand-r^{PAMmis} and Tbx1/10^{PAMmis} are resistant to the Cas9 nuclease activity. Primer sequences are listed in Supplementary Table 1.

CRISPR/Cas9-mediated loss of Hand-r function

The pair of single guide RNA (sgRNA) targeting Tbx1/10 (sgTbx1/10) has been validated previously (Tolkin and Christiaen, 2016). Rescue of the Tbx1/10 loss-of-function was achieved by TVC-specific overexpression of Tbx1/10^{PAMmis} driven by a *FoxF* enhancer (FoxF-1>Tbx1/10^{PAMmis}). For Hand-r loss of function, sgRNAs were first designed to avoid genomic off-targets and tested as described (Gandhi et al., 2017). In short, sgRNA expressing cassettes (U6>sgRNA) were assembled by single step overlap PCR. Individual PCR products (~25 µg) were electroporated with EF1a>NLS::Cas9::NLS (30µg) , Myod905>Venus (50 µg), driving ubiquitous expression of Cas9 and a widely expressed fluorescent reporter construct, respectively. Efficient electroporation was confirmed by observation of fluorescence before genomic DNA extraction around 16 hpf (18°C) using QIAamp DNA Micro kit (Qiagen, German Town, MD). Mutagenesis efficacy of individual sgRNAs, as a linear function of Cas9-induced indel frequency, was estimated from electrophoregrams following Singer sequencing of the targeted regions amplified from extracted genomic DNA by PCR. Result of the relative quantification of the indel frequency ("corrected peakshift" of 22% and 24%) was considered high enough for both sgRNAs targeting Hand-r, which were finally selected. The corresponding cassettes were cloned into plasmid for repeated electroporations to study the loss of function of Hand-r.

741 Rescue of Hand-r loss-of-function was achieved by overexpression of Hand-r^{PAMmis}
742 driven by a FoxF TVC specific enhancer (FoxF-1>Hand-r^{PAMmis}). In order to control the
743 specificity of the CRISPR/Cas9 system, sgRNAs targeting *Neurogenin*, a gene not
744 expressed in the TVC and their progeny, was electroporated in parallel. Sequences of the
745 DNA targets and oligonucleotides used for the sgRNAs are listed in Supplementary Table
746 1.
747

748 **Observation and imaging**

749 Samples were usually scored under a DM2500 epifluorescent microscope (Leica
750 Microsystems, Wetzlar, Germany). Imaging was performed using a TCS SP8 X inverted
751 confocal microscope equipped with a white light laser, AOBS and HyD detectors (Leica
752 Microsystems).
753

754 **Acknowledgement**

755 We thank Robert Kelly (Université Aix-Marseille, CNRS, France) for feedbacks on the
756 manuscript. We are grateful to Wei Wang, Nicole Kaplan, Claudia Racioppi and Alberto
757 Stolfi for collaborative inputs throughout the project. We thank Farhana Salek and
758 Kristyn Millan for technical support. This project was funded by NIH/NHLBI R01 award
759 HL108643, and trans-Atlantic network of excellence award 15CVD01 from the Leducq
760 Foundation to L.C.
761

Figures

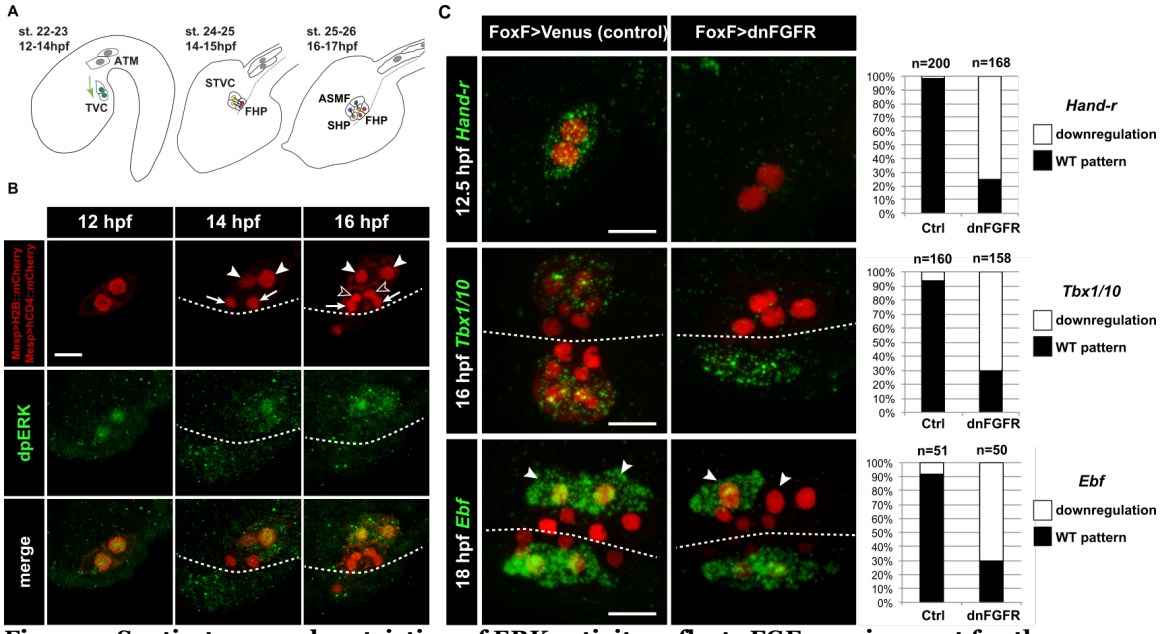

Figure 1. Spatio-temporal restriction of ERK activity reflects FGF requirement for the specification of cardiopharyngeal progenitors. (**A**) Schematic of *Ciona* development showing asymmetric cell divisions and resulting cell fates of the cardiopharyngeal mesoderm (CPM). Embryonic and larval stages (St) according to (Hotta et al., 2007) with hours post fertilization (hpf) at 18°C. Anterior tail muscle (ATM, gray), trunk ventral cell (TVC, green), secondary TVC (STVC, green), first heart precursor (FHP, red), second heart precursor (SHP, orange), atrial siphon founder cell (ASMF, blue). Black bars link sister cells. Dashed lines: ventral midline. The first stage presents a quasi-lateral view while the second and third stages present quasi-ventral views. Anterior is to the left. Scale bar, 50 µm. (**B**) ERK activity visualized by anti-dpERK antibody (green). TVCs and their progeny are marked by mCherry driven by *Mesp* and revealed by anti-mCherry antibody (red). H_2B::mCherry and hCD4::mCherry accumulate in the nuclei and at the cell membrane, respectively. Arrowheads indicate STVCs and ASMFs at 14 and 16 hpf, respectively. Arrows indicate FHPs and open arrowheads mark SHPs. Anterior to the left. Scale bar, 10 µm. See also Figure S1 for broader time series of dpERK immunostaining in the B7.5 lineage. (**C, D**) TVC-specific overexpression of dnFGFR induces loss of expression of key lateral CPM markers visualized by *in situ* hybridization. (**C**) Representative expression patterns of key CPM genes (*Hand-related*, *Tbx1/10*, *Ebf*) in control embryos (control, electroporated with FoxF(TVC):bpFOG-1>Venus) and TVC-specific dnFGFR expression (electroporated with *FoxF(TVC):bpFOG-1>dnFGFR::mCherry*) individuals. TVCs and progeny are marked with *Mesp>NLS::lacZ* (red). Loss of expression in half of the TVC progeny, as presented for *Ebf*, is assumed to be due to left-right mosaicism. Arrowheads mark the ASMFs. Anterior is to the left. Scale bar, 10 µm. (**D**) Corresponding histograms with the phenotype proportions. For simplicity, loss of gene expression in half or all of the TVCs and their progeny were combined in the same category. "n" corresponds to the number of individual halves documented per condition.

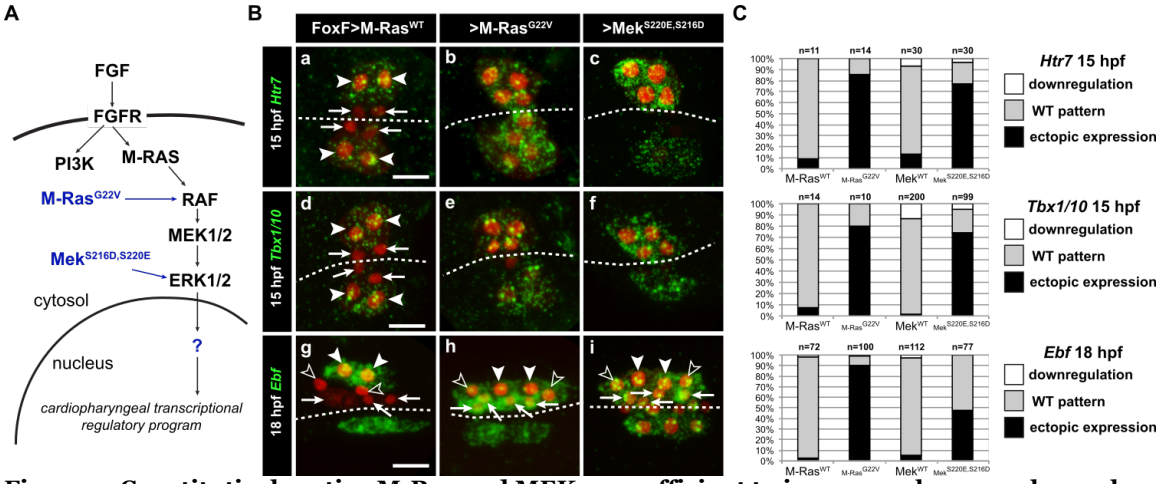

Figure 2. Constitutively active M-Ras and MEK are sufficient to impose a pharyngeal muscle fate in the cardiopharyngeal lineage. (**A**) Diagram of the FGF/MAPK transduction pathway with constitutive activation by M-Ras^{G22V} and MEK^{S216D,S220E} mutants. (**B**) Expression patterns of markers of the lateral TVC progeny, *Htr7* (a, b, c,), *Tbx1/10* (d, e, f) and *Ebf* (g, h, i), visualized by *in situ* hybridization following TVC-specific over-expression of M-Ras^{WT} (as control), M-Ras^{G22V} and MEK^{S216D,S220E}. M-Ras^{WT} overexpression (a, d, g) does not alter the wild-type spatial expression patterns of *Htr7*, *Tbx1/10* and *Ebf* in lateral TVC derivatives (STVC and ASMF) and excluded from the median heart precursors. TVC-specific over-expression of M-Ras^{G22V} (b, e, h) or MEK^{S216D,S220E} (c, f, i) induces ectopic expression of STVC and/or ASMF markers (*Htr7*, *Tbx1/10* and *Ebf*) in the more median cells, that normally form cardiac precursors. Solid arrowheads indicate STVCs and ASMFs at 15 and 18 hpf, respectively. Arrows indicate FHPs and open arrowheads mark SHPs. At 18 hpf, the FHPs start dividing or have divided into 4 cells. Anterior to the left. Scale bar, 10 µm. (**C**) Corresponding histograms: Larvae with TVC-specific over-expression of MEK^{WT} retain the wild-type expression patterns. For simplicity, ectopic expressions in half to all of the cardiac precursors were combined in the same phenotype category. "n" corresponds to the number of embryo halves documented per condition. See also Figure S2.

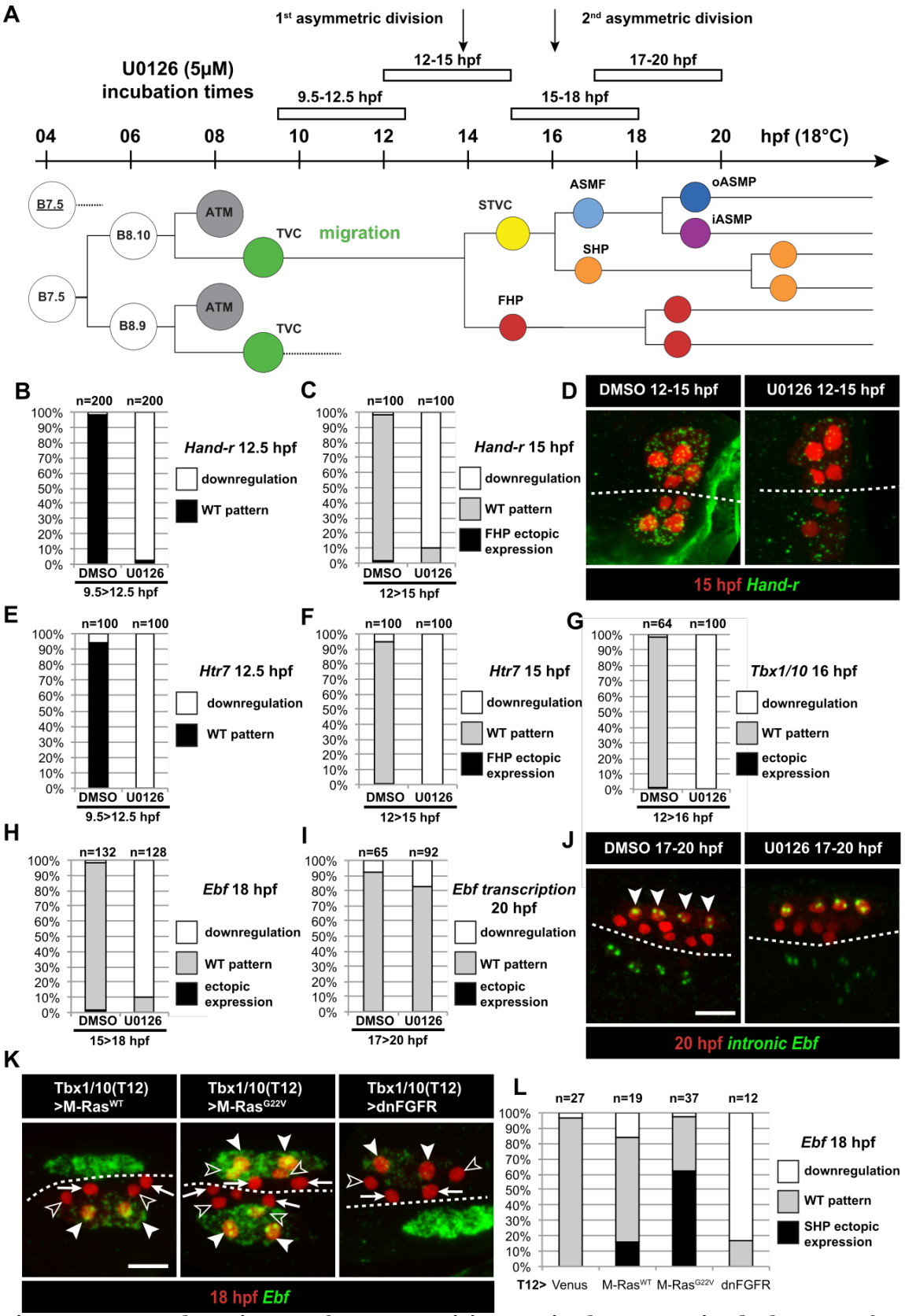

Figure 3. Temporal requirement for MAPK activity permits the progressive deployment of the cardiopharyngeal regulatory program. (**A**) Summary of the CPM cell lineage showing the

different U0126 treatments with regard to the timing of the cell divisions. Abbreviations and color codes as in Figure 1. (**B, C**) Proportions of embryo halves with wild-type or downregulated expression of *Hand-r* at 12.5 hpf (B) and 15 hpf (C) following 3-hour incubations in U0126 (with DMSO as control treatment). (**D**) *Hand-r* expression visualized by *in situ* hybridization at 15 hpf in control (DMSO treated) and U0126 treated embryos. In control embryos, *Hand-r* remains expressed in the STVCs and downregulated in the FHPs. In U0126 (12-15 hpf) treated embryos, downregulation of *Hand-r* expression is observed throughout the TVC progeny (STVCs and FHPs), suggesting inhibition of transcription and inheritance of remnant transcripts following TVC divisions. (**E, F**) Proportions of embryo halves with wild-type or downregulated expression of *Htr7* at 12.5 hpf (E) and 15 hpf (F) following 3-hour incubations in U0126 (with DMSO as control treatment). (**G**) Proportions of larvae with wild-type expression or downregulated expression of *Tbx1/10* at 16 hpf following 4-hour incubation in U0126 (with DMSO as control). (**H**) Proportions of larvae with wild-type or downregulated expression of *Ebf* at 18 hpf following a three hour incubation in U0126 (with DMSO as control). (**I**) Proportions of larvae with wild-type or downregulated transcription of *Ebf* at 18 hpf following a 3-hour incubation in U0126 (DMSO as vehicle control). (**J**) Pattern of nascent *Ebf* transcripts visualized by *in situ* hybridization with intronic probes (green) at 20 hpf. The nuclear dots reveal the active transcription sites in the four ASMPs per side in larvae, both control/DMSO- and U0126-treated from 17 to 20 hpf. (**K**) *Ebf* expression (green) in 18hpf larvae expressing control M-Ras^{WT}, constitutively active M-Ras^{G22V} or dominant negative dnFGFR under the control of the T12 element, an STVC-specific *Tbx1/10* enhancer. Arrows: first heart precursors (FHP); open arrowhead: second heart precursors (SHPs); closed arrowheads: ASM founder cells (ASMFs); dotted line: midline. (**L**) Proportions of larvae with wild-type or downregulated expression of *Ebf* at 18 hpf in larvae with Venus (control), M-Ras^{WT}, M-Ras^{G22}, or dnFGFR driven by *Tbx1/10 cis*-regulatory sequence and overexpressed in the STVCs. "n" : number of individual halves documented per condition.

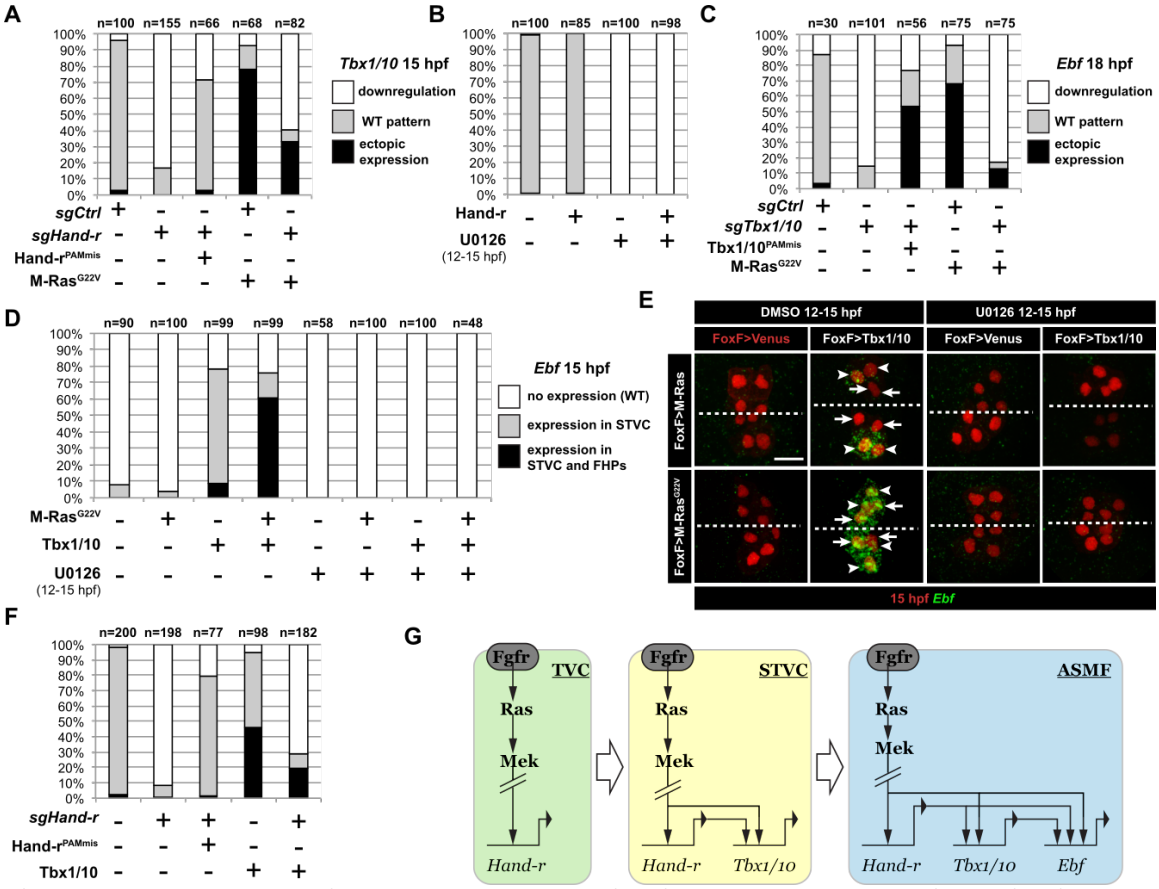

Figure 4. M-Ras/MAPK-driven feed-forward subcircuits control the successive activations of *Hand-r*, *Tbx1/10* and *Ebf*. (**A**) Proportions of embryo halves with indicated *Tbx1/10* expression patterns following TVC-specific CRISPR/Cas9-mediated mutagenesis of *Neurogenin/Neurog* as a control (*sgCtrl*), and Hand-r (*sgHand-r*). TVC-specific overexpression of a CRISPR/Cas9-resistant form of Hand-r with mutation in the PAM sequence (*Hand-r*^{PAMmis}) rescued *Tbx1/10* expression in the *sgHand-r* "background". TVC-specific overexpression of a constitutively active M-Ras mutant (M-Ras^{G22}) (control: M-Ras^{WT}) was sufficient to induce ectopic expression of *Tbx1/10* in the FHPs in *sgCtrl* embryos but not in *sgHand-r* embryos indicating that Hand-r is necessary for M-Ras-dependent activation of *Tbx1/10* transcription. (**B**) Proportions of embryo halves with indicated *Tbx1/10* expression patterns following TVC-specific overexpression of Hand-r or a neutral reporter (Venus) and treated from 12 to 15hpf with the MEK inhibitor U0126 (+) or with DMSO (-) as control. Hand-r overexpression is not sufficient to rescue loss of *Tbx1/10* expression due to MAPK inhibition indicating that M-Ras/MAPK activity is required in parallel of Hand-r expression to activate Tbx1/10 transcription in the TVC progeny. (**C**) Tbx1/10 is necessary downstream of M-Ras/MAPK activity to activate *Ebf* transcription in the TVC progeny. Shown are proportions of *Ebf* expression phenotypes following TVC-specific CRISPR/Cas9-mediated loss of *Tbx1/10* function (*sgTbx1/10*), with *Neurog*-targeting sgRNA as control (*sgCtrl*). Specificity of Tbx1/10 loss of function was validated through rescue of *Ebf* expression with TVC-specific overexpression of a CRISPR/Cas9 resistant form of *Tbx1/10* (Tbx1/10^{PAMmis}). Ectopic *Ebf* expression in SHPs in Tbx1/10^{PAMmis} larvae is explained by precocious misexpression of Tbx1/10 in the TVC as described in Wang et al, 2013. TVC-specific overexpression of M-Ras^{G22} (M-Ras^{G22}), with wild type M-Ras (M-Ras^{WT}) as control, was sufficient to induce ectopic expression of *Ebf* in the cardiac precursors in *sgCtrl* embryos but not in *sgTbx1/10* embryos indicating that Tbx1/10 is necessary for M-Ras-dependent activation of *Ebf* transcription. (**D, E**) Proportions (D) and examples (E) of 15hpf larvae halves showing indicated *Ebf* expression phenotypes in *sgCtrl* and *sgHand-r* CRISPR/Cas9 conditions combined with TVC-specific overexpression of a neutral reporter (Venus), Hand-r^{PAMmis}, or Tbx1/10, and with MEK inhibition by U0126 (+) or not (DMSO control (-)). Arrowhead: STVCs, Arrows: FHPs, dotted line: ventral midline (**F**) Loss of Hand-r function impaired the ability of Tbx1/10 to induce ectopic *Ebf* expression. For simplicity, ectopic expressions in half to all of the cardiac precursors were combined in the same phenotype category. "n": number of individual halves documented per condition. (**G**) Summary model of the temporal deployment of FGF/MAPK-driven feed-forward subcircuits leading to the sequential activations of *Tbx1/10* and *Ebf* in the STVCs and ASMFs, respectively.

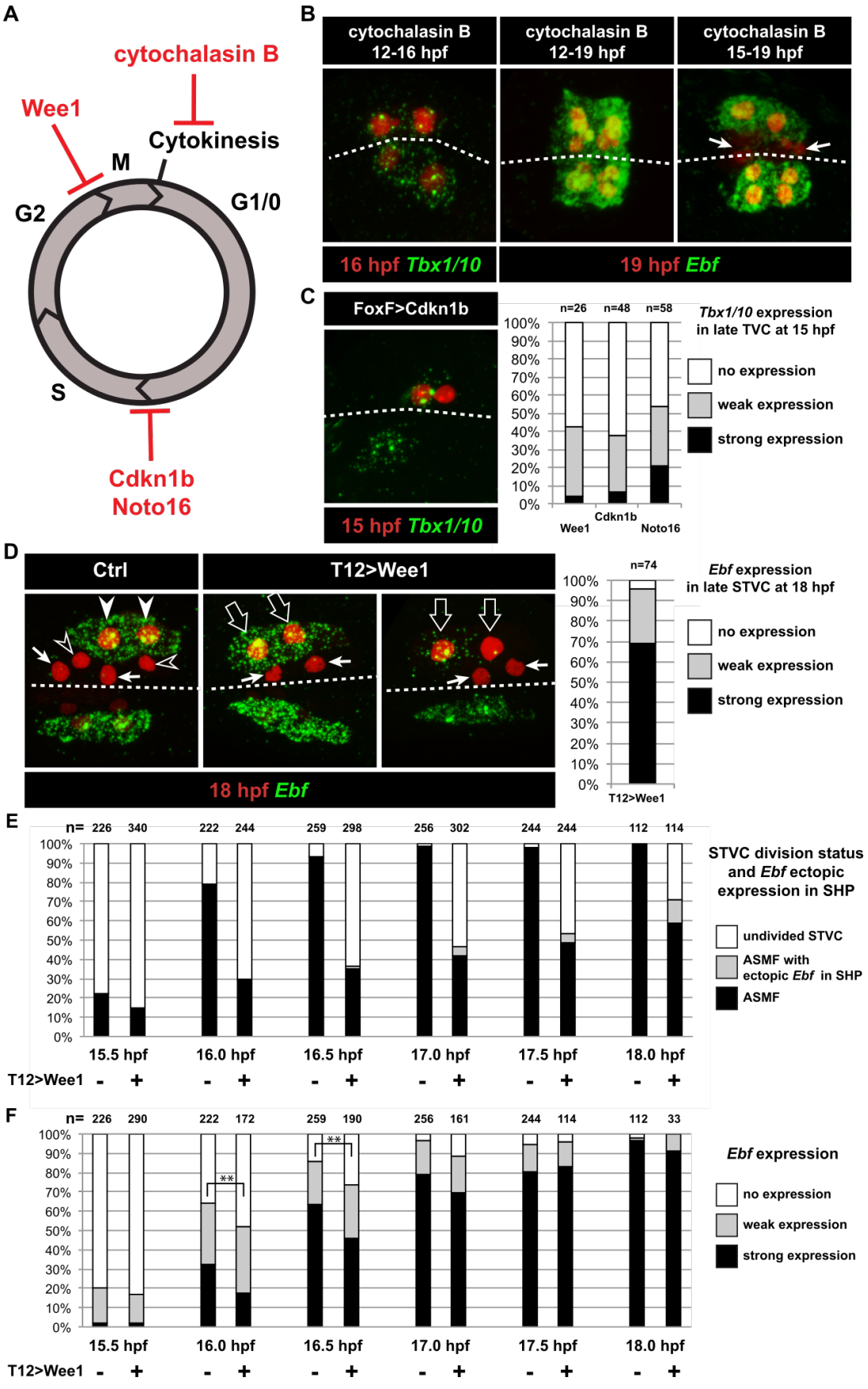

863

Figure 5. Temporal deployment of the cardiopharyngeal network is partially coupled with cell cycle progression. (**A)** Schematic representation of the canonical eukaryotic cell cycle, and actions of the perturbations used in this study. (**B**) Tbx1/10 and Ebf expression at indicated time points, and following inhibition of cytokinesis by cytochalasin B treatment at indicated time points. Note that 15 to 19hpf treatment is applied AFTER the first division and birth the FHPs, which do not activate *Ebf* at 19hpf (right panel, arrows). (**C**) Inhibition of G1/S or G2/M blocks TVC division, and reduces *Tbx1/10* expression. Picture shows left-right mosaic embryo, with TVCs that have not divided on the electroporated side (marked by *Mesp>H2B::mCherry*, red), one cell turned on Tbx1/10, but not the other. Left: the proportions of embryos showing strong Tbx1/10 expression is substantially reduced compared to control embryos (e.g. Figure 1, and (Wang et al., 2013)). (**D**) Inhibition of G2/M in the STVCs by misexpression of Wee1 using the *Tbx1/10 T12* enhancer inhibits STVC division, and has a mild impact on *Ebf* expression at 18hpf. Open arrows indicate STVCs that have not divided, but express high (middle) or low (right) levels of *Ebf*. Left: control larva showing high *Ebf* expression in the ASMF (closed arrowheads), but neither in the SHPs (open arrowheads) nor in the FHPs (Arrows). (**E**) Proportions of larva halves fixed at successive time points and showing undivided STVCs, or ASMFs with or without ectopic *Ebf* expression in the SHPs following STVC-specific expression of the G2/M inhibitor Wee1 (+), or a control construct (-). See Figure S4C for an example of ectopic *Ebf* expression in the SHPs (grey labels). Note the sharp increase in % of larva with ASMF between 15.5 and 16hpf, indicating that mitosis occurs primarily during this time window, but is delayed in a majority of larvae upon Wee1 misexpression. (**F**) Proportions of larva halves with cells showing indicated Ebf expression. The numbers (n) for cells expressing Wee1 focus on cells that have not divided (% shown in E), to estimate the dynamics of *Ebf* activation in G2/M-inhibited cells. Control cells consist mostly ASMFs after 15.5hpf as shown in (E). Wee1 and controls distributions differ significantly only at 16 and 16.5hpf (**, $p<0.01$, Chi^2 test), suggesting that Wee1 merely delays the accumulation of Ebf transcripts. In all image panels, dotted line : ventral midline.

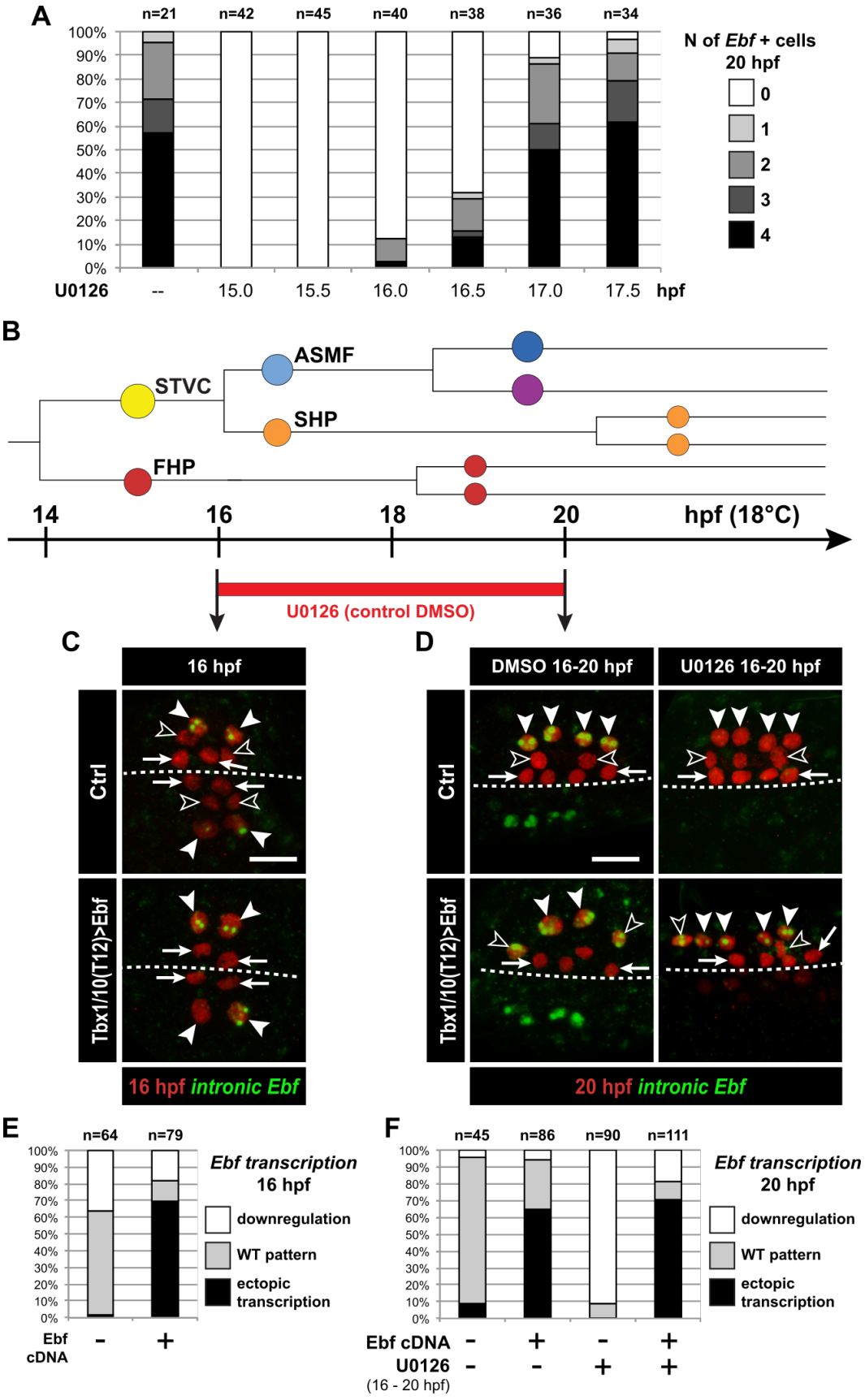

889

Figure 6. *Ebf* regulation transitions from MAPK-dependent to autoregulative during the early phase of ASMF cycle. (**A**) Proportions of 20hpf larva halves showing the indicated number of Ebf-expressing cells following U0126 treatments started at the indicated time points. This indicates that, by 17hpf, Ebf expression, which started at ~16hpf, has become largely insensitive to loss of MAPK activity. (B) Summary lineage diagram and time scale indicating the approximate stages for U0126 and DMSO (control) treatments for the results shown in (C, D). (C) Control (Ctrl) and Ebf-misexpressing embryos fixed at 16hpf, prior to chemical treatments, and stained for nascent transcripts with an intronic *Ebf* probe. In controls, the ASMFs (solid arrowhead), but neither the SHPs (open arrowheads) nor the FHPs (arrows), actively transcribe *Ebf* (green nuclear dots). In Larvae misexpressing the Ebf cDNA under the control of the STVC-specific Tbx1/10 enhancer, divisions are delayed and STVCs (solid arrowheads) activated transcription of endogenous *Ebf* loci (green nuclear dots). (D) After 4 hours, U0126 treated ASMFs no longer transcribe Ebf (top right image, solid arrowheads), whereas control DMSO-treated ASMFs do (top left, green nuclear dots). Upon misexpression of the Ebf cDNA in the STVCs and derivatives, ongoing *Ebf* transcription is detected at 20hpf in both DMSO and U0126-treated cells, and it persists in both ASMFs (solid arrowheads), and SHPs (open arrowheads). (**E, F**). Proportions of larvae halves showing the indicated *Ebf* transcription patterns, in indicated experimental conditions, as illustrated in C and D, respectively.

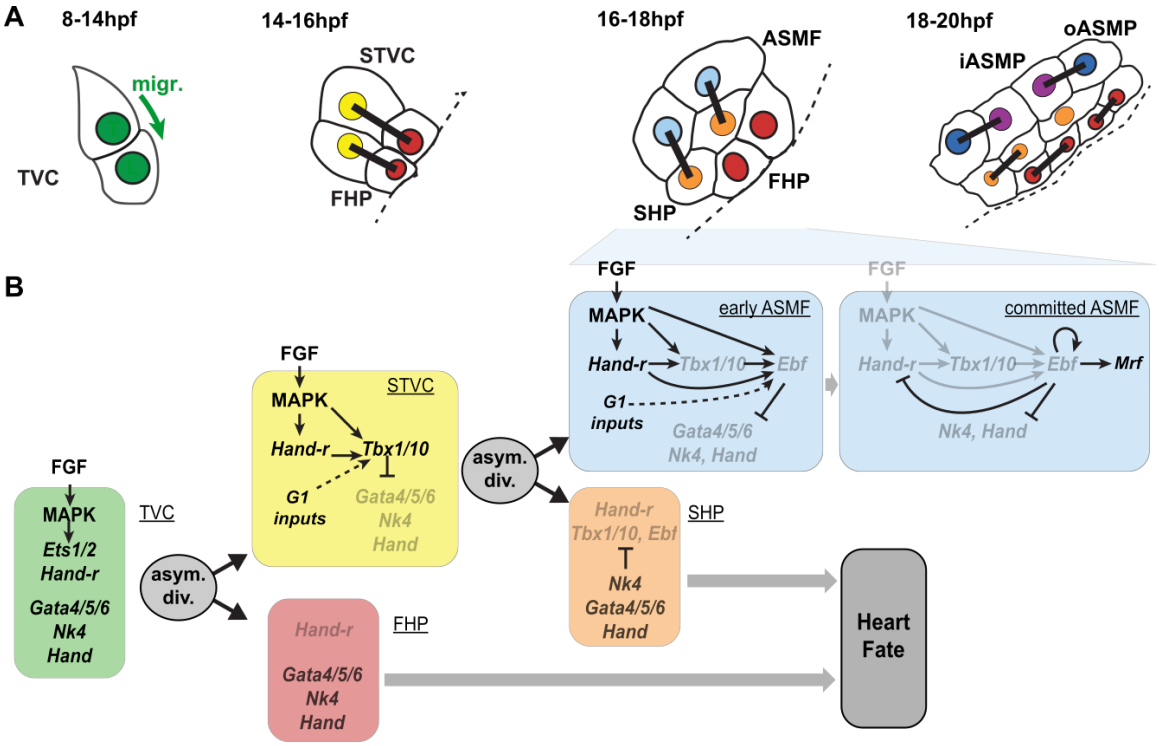

Figure 7. Summary model. (**A**) Schematic representation of cardiopharyngeal lineage cells at successive time points representing the main fate transitions. hpf: hours post-fertilization; TVC: trunk ventral cells; L: Leader T: trailer; migr.: migration; STVC: second trunk ventral cells; FHP: first heart precursors; dotted line: midline; black bars link sister cells; ASMF: atrial siphon muscle founder cells; SHP: second heart precursors; iASMP: inner atrial siphon muscle precursors; oASMP: outer atrial siphon muscle precursor (these cells correspond to stem-cell-like *Mrf*-; Notch+ precursors and *Mrf*+; Notch- differentiating myoblasts, respectively; see (Razy-Krajka et al., 2014) for details). (**B**) Lineage diagram and documented regulatory relationships between indicated genes and pathways, as showing here and in (Razy-Krajka et al., 2014; Wang et al., 2013). In TVCs, primed heart and ASM markers are coexpressed, and maintenance of the STVC and ASM markers requires ongoing FGF/MAPK signaling. Following the first oriented and asymmetric cell division, FGF/MAPK is maintained only in the STVCs, which permits the continued expression of Hand-r and the activation of *Tbx1/10*. Cell division, presumably through G1-specific inputs, contributes to *Tbx1/10* activation, and Tbx1/10 function antagonizes *Gata4/5/6* expression (Wang et al., 2013). In the FHPs, termination of FGF/MAPK signaling inhibits *Hand-r* expression and prevents *Tbx1/10* activation. Following oriented and asymmetric division of the STVCs, FGF/MAPK signaling persists only in the ASMFs, where it permits the transient maintenance of *Hand-r* and *Tbx1/10*, both of which act in parallel to FGF/MAPK to activate *Ebf* expression, together with contributions from presumed G1 inputs. Ebf activities further antagonize the cardiac program (marked by *Gata4/5/6*, *Nk4/Nkx2-5* and *Hand* expression; (Razy-Krajka et al., 2014; Stolfi et al., 2010; Wang et al., 2013)). Once Ebf expression reaches "high levels", its regulation becomes MAPK-independent and self-activating (this study). It also feeds back negatively on early activators such as Hand-r, and promotes the expression of the muscle determinant *Mrf* (Razy-Krajka et al., 2014; Tolkin and Christiaen, 2016). We propose that this transition represents commitment to an ASM fate. In the SHPs, termination of FGF/MAPK signaling prevents maintenance of Hand-r and Tbx1/10 expression, which, together with repressive inputs from Nk4/Nkx2-5, inhibits *Ebf* activation (Wang et al., 2013), and permits heart fate specification (Wang et al., 2017).

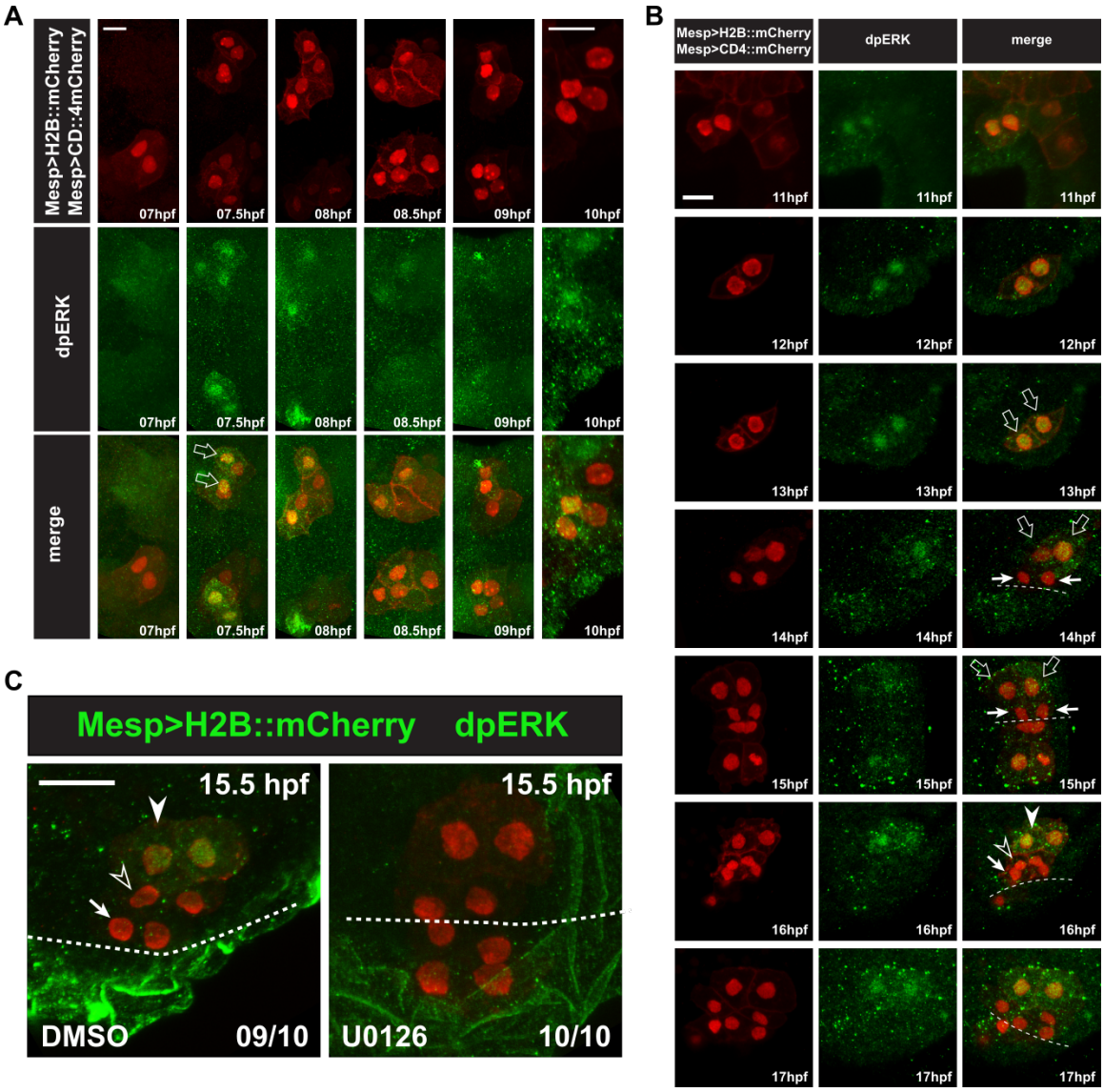

Figure S1. Detailed patterns of MAPK activity during early cardiopharyngeal development. (**A**) MAPK activation during TVC induction. Close-up views of B7.5 lineage cells marked with Mesp>H2B::mCherry (nuclei) and Mesp>hCD4::mCherry (membranes) and immunostained for dpERK at indicated successive time points between 7 and 10hpf. DpERK staining was not detected in the founder cells at 7hpf, but increased sharply and specifically in the smaller trunk ventral cells (TVCs, open arrows) at 7.5hpf, but not in the larger anterior tail muscles (ATMs). DpERK staining persisted throughout TVC migration (see also B). (B) MAPK activation patterns during cardiopharyngeal fate diversification. DpERK staining was clearly detected in migrating TVCs (open arrows, 11 to 13hpf); in lateral large STVCs (open arrows, 14 to 15hpf), but not in the small median first heart precursors (FHPs, arrows, 14 to 15hpf); in the large lateral atrial siphon muscle founder cells (ASMFs, solid arrowheads, 16 to 17hpf), but neither in the FHPs (arrows), nor in the second heart precursors (SHPs, open arrowheads). **(C)** Treatment with the MEK inhibitor U0126 between abolished dpERK staining in the lateral STVCs, compared to a control treatment with DMSO. Numbers of embryos showing the presented pattern out of the total numbers of embryos are shown.

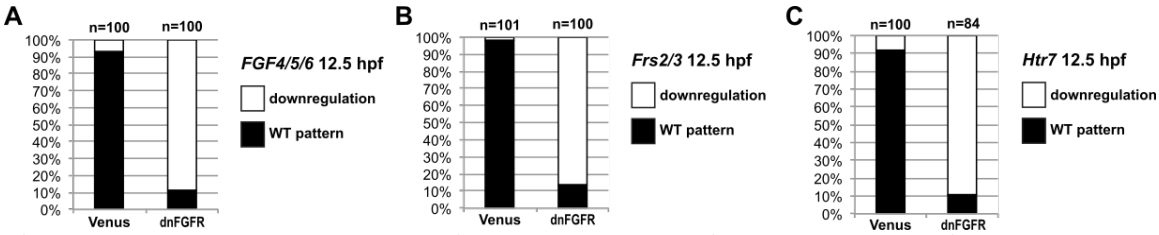

Figure S2. Other markers expressed in the TVC need continuous FGF/MAPK inputs for maintenance. All panels show the proportions of 12.5hpf embryos halves showing expression of the indicated genes in late TVCs, following electroporation of either a FoxF(TVC)>Venus control of a FoxF(TVC)>dnFGFR construct that inhibits signaling through FGFR. Wild-type pattern were first reported in (Razy-Krajka et al., 2014).

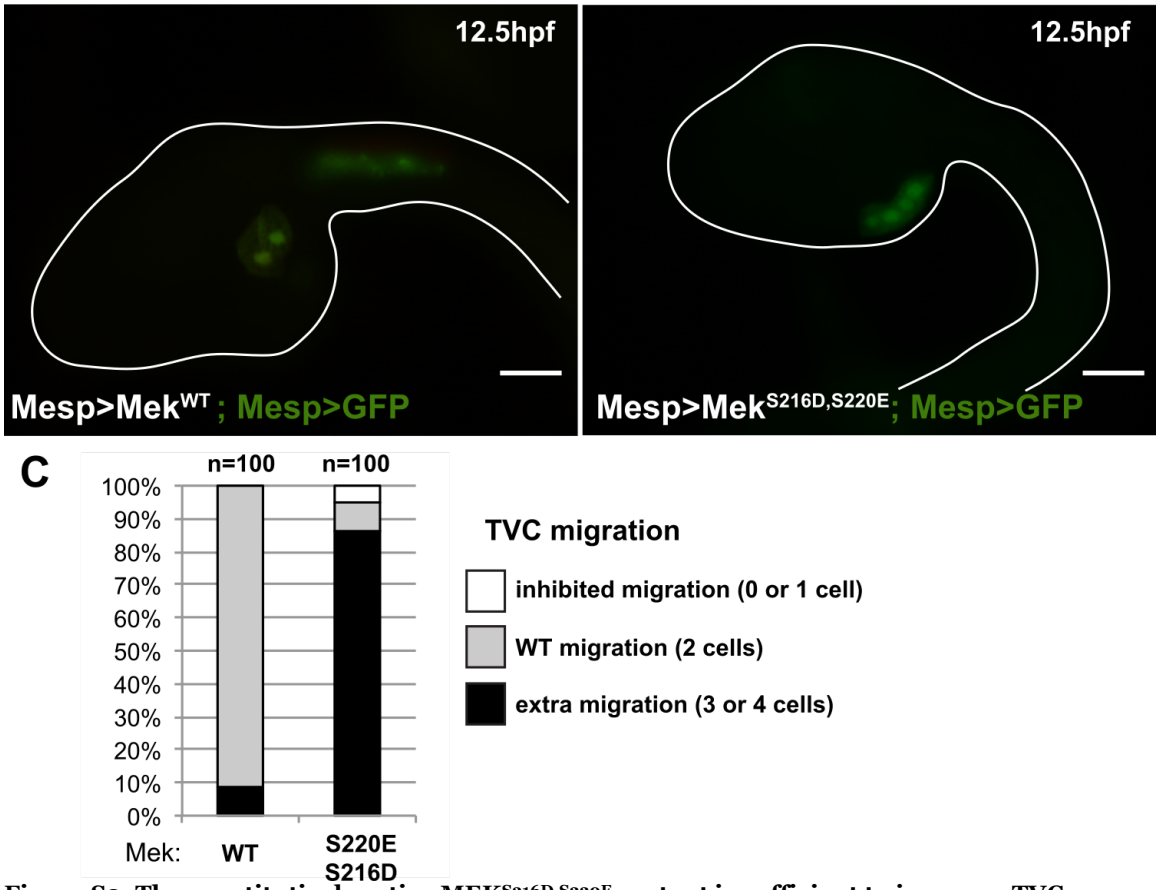

Figure S3. The constitutively active MEK^{S216D,S220E} mutant is sufficient to impose a TVC identity to the whole B7.5 lineage. (A) Control late tailbud embryo showing the left side B7.5 lineage expressing GFP and a MEK^{WT} control under the control of the *Mesp* enhancer. Two TVCs and two ATMs are normally induced, and TVCs migrated into the trunk. (B) Late tailbud embryo showing the left side B7.5 lineage expressing GFP and a MEK^{S216D,S220E} mutant under the control of the *Mesp* enhancer. Four cells are observed as having migrated into the trunk, indicating that they have been induced to acquire a TVC fate and migrate, replicating FGF/MAPK gain-of-function phenotypes as described in (Davidson et al., 2006). (C) Proportions of embryo halves showing the indicated phenotypes. Extra migration is interpreted as ectopic induction of the TVC fate in all B7.5 lineage cells. Scale bar ~ 20μm.

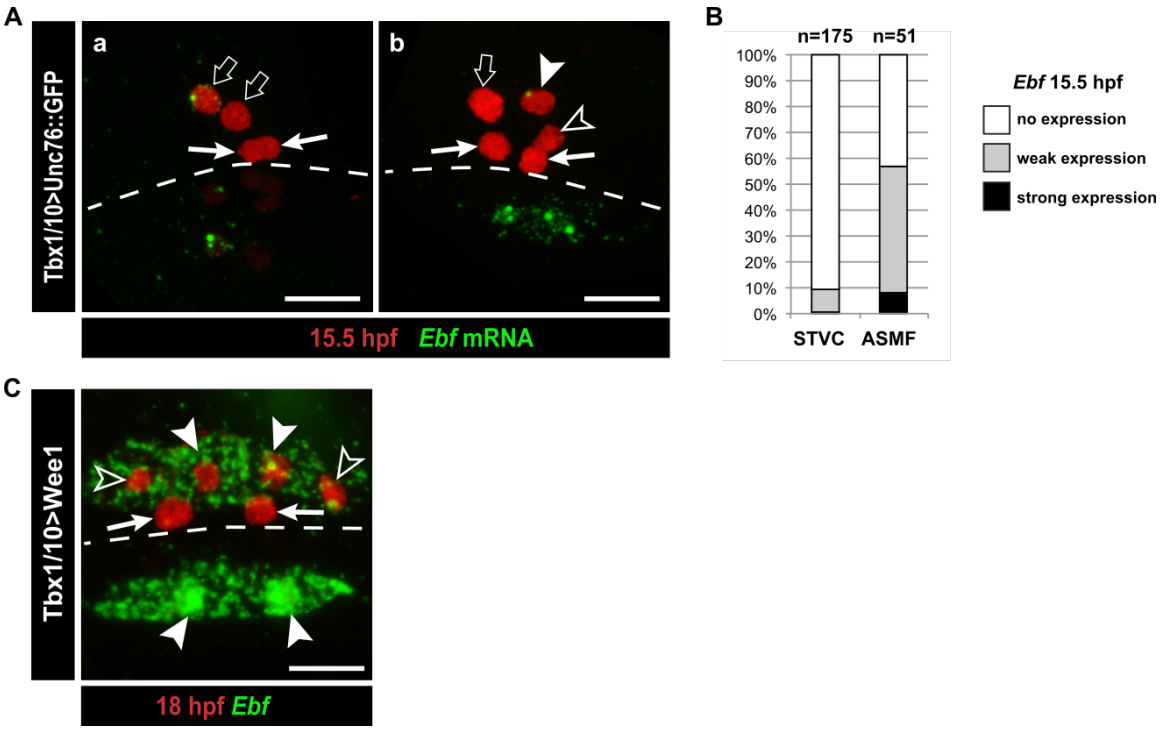

Figure S4. Rare precocious activation of *Ebf* transcription in STVCs. (**A**) 15.5hpf Cardiopharyngeal lineage cells expressing Mesp>H2B::mCherry (red) and control Tbx1/10>unc76::GFP construct (not visible). (**A.a**) Green nuclear dot indicates nascent Ebf transcription in an STVC (open arrow), but not the other, and not in the first heart precursors (FHP; arrow). (A.b) left pair of nuclei shows an STVC (open arrow) and an FHP (arrow), neither of which express *Ebf*, whereas the cousin ASMF (solid arrowhead) shows nascent *Ebf* transcription (green dot). Dotted line : midline. (**B**) Proportions of STVCs and ASMFs showing indicated *Ebf* expression patterns. Note that >90% of STVCs do not express *Ebf*, which turns on almost exclusively in ASMFs. (**C**) Cardiopharyngeal lineage cells with *Ebf* expression in the ASMFs (solid arrowheads), and ectopically in the SHP (open arrowheads), but not in the FHPs (arrows), following misexpression of Wee1 using the STVC-specific *Tbx1/10 T12* enhancer. Dotted line: midline.

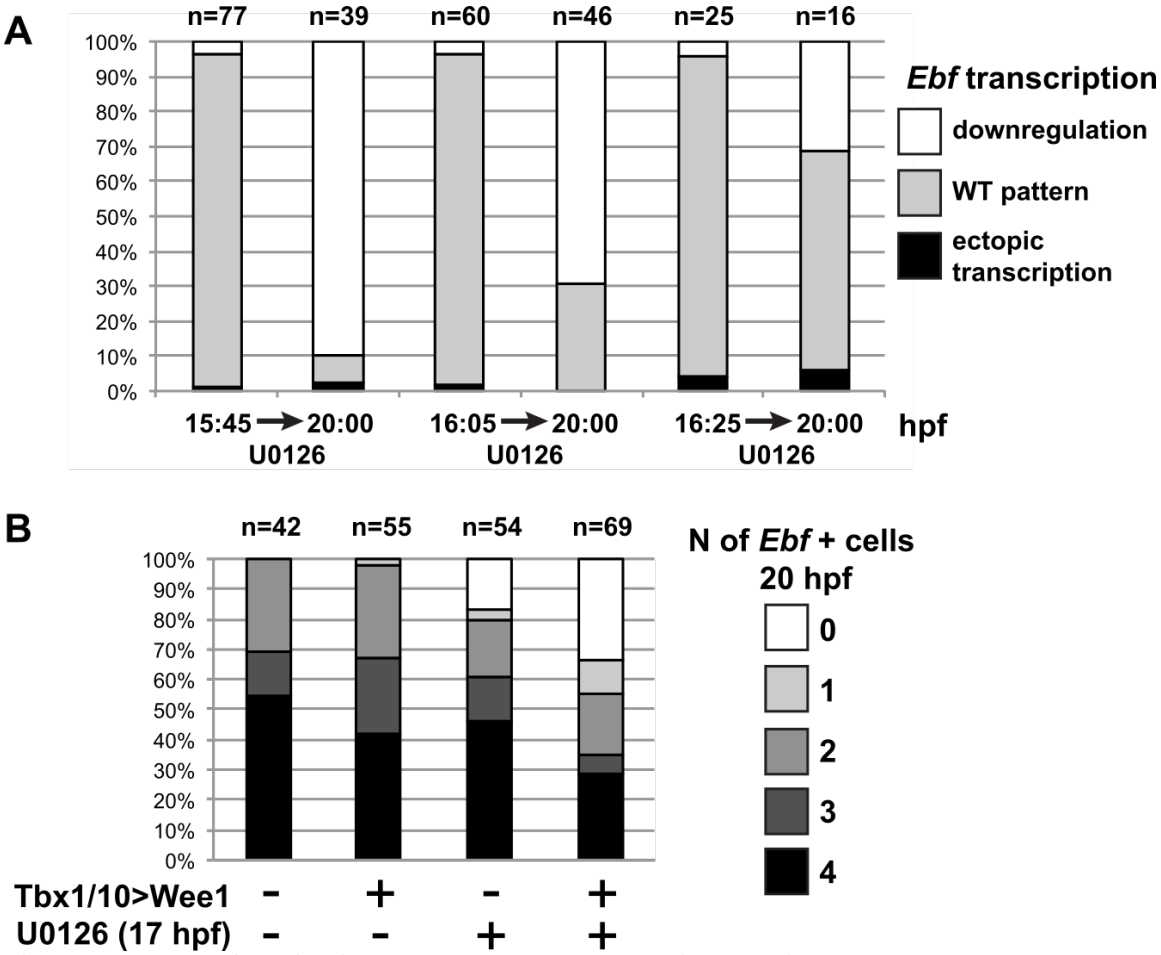

Figure S5. MAPK signaling is necessary for *Ebf* expression only in early ASMF, and cell cycle inputs shorten the MAPK-dependent period. (**A**) Proportions of larva halves showing the indicated *Ebf* transcriptional activity (assayed using intronic probes). Batches of larvae expressing *Mesp>H2B::mCherry* were split to be fixed for WMFISH or treated with U0126 at 3 successive time points (15.75hpf, 16hpf or 16.25hpf), and the treated larvae were fixed at 20hpf. This data shows that, although all batches expressed *Ebf* at the beginning of the experiment, only when MEK was inhibited later (16.25hpf) did *Ebf* transcription persist in 20hpf larvae. (**B**) Proportions of larva halves showing the indicated numbers of *Ebf*+ cells at 20hpf, following expression of the G2/M inhibitor Wee1 in the STVCs, under the control of the *Tbx1/10 T12* enhancer (+). Negative controls (-) were electroporated with a *Tbx1/10(T12)>Venus* construct. Larvae were also treated with U0126 (+) or DMSO (as negative control, (-)), starting at 17hpf, which corresponds to the transition from a MAPK-dependent to a MAPK-independent autoregulative mode of *Ebf* expression (see Figure 6A). Wee1-induced delays in cell cycle progression increased the sensitivity of late *Ebf* expression to MAPK inhibition, further supporting the notion that cell divisions accelerate the transition from MAPK-dependent to MAPK-independent self-activating regulation of *Ebf* transcription.

Primer name	primer sequence
MRAS N FWD INF bpFOG-1	cacacaaGCGGCCGCaaccATGGCGACCGTGCCGAATC
MRAS C REV INF EcoR1	gctcagctggaattcTGGCCTCTAGGTGGAGCTAC
MRAS G22V TOP	GTGGTTGGCGATGTTGGTGTCGGGAAG
MRAS G22V BOT	CTTCCCGACACCAACATCGCCAACCAC
MEK1/2 N FWD Not1	caaGCGGCCGCaaccATGCCTCCTAAACGTAAGT
MEK1/2 C REV Ecor1	ctggaattcCCCATCATATTAATCAGGTACA
MEK MUT R	CCCTACAAACTCGTTGGCCATATCGTCGATCAGTTGCCCGCTCA
MEK MUT F	CTGATCGACGATATGGCCAACGAGTTTGTAGGGACAAGATCATA
Noto16 FWD INF bpFOG-1	acacacaaGCGGCCGCaaccATGGTTCCCCCACCTTCGTAC
Noto16.2 REV INF EcoR1	GCTCAGCTGGAATTCATTTTCGTATCAATTACTTGCTTTGG
Cdkn1B FWD INF bpFOG-1	acacacaaGCGGCCGCaaccATGGCGGACAAAAAACCCCCG
Cdkn1B REV INF EcoR1	gctcagctggaattcCGTGGCACAGTATGACGTCAC
Tbx1 G325A Mut Top	CGGCTCCGTGGAGAAGAAAATGAGCG
Tbx1 G325A Mut Bot	CGCTCATTTTCTTCTCCACGGAGCCG
Tbx1 G579A Mut Top	GAAAGATTGGTGGCCGTAGAAGCAAAACTGGAAATG
Tbx1 G579A Mut Bot	CATTTCCAGTTTTGCTTCTACGGCCACCAATCTTTC
Hand-r C153T Mut Top	CTTTGCAACCGAAAATCCACACATGGTAGC
Hand-r C153T Mut Bot	GCTACCATGTGTGGATTTTCGGTTGCAAAG
Hand-r C574T Mut Top	GTCGCGTCCGAGTCATCCGTATTATCACTTC
Hand-r C574T Mut Bot	GAAGTGATAATACGGATGACTCGGACGCGAC

		final sgRNA
sgHandR.3.aFwd	GAGGCCCTGCTACCATGTGTGTTTAAGAGCTATGCTGGAAACAG	GAGGCCCTGCTACCATGTGT
sgHandR.3.cFwd	GAGGTTCGAAGTGATAATACGTTTAAGAGCTATGCTGGAAACAG	GAGGTTCGAAGTGATAATAC
sgHandR.3.aRev	ACACATGGTAGCAGGGCCTCatctataccatcggatgccttc	GAGGCCCTGCTACCATGTGT
sgHandR.3.cRev	GTATTATCACTTCGAACCTCatctataccatcggatgccttc	GAGGTTCGAAGTGATAATAC

Table S1. oligonucleotides sequences

REFERENCES

Abu-Issa, R., Smyth, G., Smoak, I., Yamamura, K., Meyers, E.N., 2002. Fgf8 is required for pharyngeal arch and cardiovascular development in the mouse. Development 129, 4613-4625.

Aggarwal, V.S., Liao, J., Bondarev, A., Schimmang, T., Lewandoski, M., Locker, J., Shanske, A., Campione, M., Morrow, B.E., 2006. Dissection of Tbx1 and Fgf interactions in mouse models of 22q11DS suggests functional redundancy. Human molecular genetics 15, 3219-3228.

Alsan, B.H., Schultheiss, T.M., 2002. Regulation of avian cardiogenesis by Fgf8 signaling. Development 129, 1935-1943.

Barron, M., Gao, M., Lough, J., 2000. Requirement for BMP and FGF signaling during cardiogenic induction in non-precardiac mesoderm is specific, transient, and cooperative. Developmental dynamics : an official publication of the American Association of Anatomists 218, 383-393.

Beh, J., Shi, W., Levine, M., Davidson, B., Christiaen, L., 2007. FoxF is essential for FGF-induced migration of heart progenitor cells in the ascidian Ciona intestinalis. Development 134, 3297-3305.

Bertrand, V., Hudson, C., Caillol, D., Popovici, C., Lemaire, P., 2003. Neural tissue in ascidian embryos is induced by FGF9/16/20, acting via a combination of maternal GATA and Ets transcription factors. Cell 115, 615-627.

Bondue, A., Lapouge, G., Paulissen, C., Semeraro, C., Iacovino, M., Kyba, M., Blanpain, C., 2008. Mesp1 acts as a master regulator of multipotent cardiovascular progenitor specification. Cell stem cell 3, 69-84.

Bothe, I., Tenin, G., Oseni, A., Dietrich, S., 2011. Dynamic control of head mesoderm patterning. Development 138, 2807-2821.

Brand, T., 2003. Heart development: molecular insights into cardiac specification and early morphogenesis. Developmental biology 258, 1-19.

Brown, C.B., Wenning, J.M., Lu, M.M., Epstein, D.J., Meyers, E.N., Epstein, J.A., 2004. Cre-mediated excision of Fgf8 in the Tbx1 expression domain reveals a critical role for Fgf8 in cardiovascular development in the mouse. Developmental biology 267, 190-202.

Buckingham, M., Vincent, S.D., 2009. Distinct and dynamic myogenic populations in the vertebrate embryo. Current opinion in genetics & development 19, 444-453.

Cai, C.L., Liang, X., Shi, Y., Chu, P.H., Pfaff, S.L., Chen, J., Evans, S., 2003. Isl1 identifies a cardiac progenitor population that proliferates prior to differentiation and contributes a majority of cells to the heart. Developmental cell 5, 877-889.

Chan, S.S., Hagen, H.R., Swanson, S.A., Stewart, R., Boll, K.A., Aho, J., Thomson, J.A., Kyba, M., 2016. Development of Bipotent Cardiac/Skeletal Myogenic Progenitors from MESP1+ Mesoderm. Stem cell reports 6, 26-34.

1038 Chan, S.S., Shi, X., Toyama, A., Arpke, R.W., Dandapat, A., Iacovino, M., Kang, J., Le,
1039 G., Hagen, H.R., Garry, D.J., Kyba, M., 2013. Mesp1 patterns mesoderm into cardiac,
1040 hematopoietic, or skeletal myogenic progenitors in a context-dependent manner. Cell
1041 stem cell 12, 587-601.

1042 Chen, L., Fulcoli, F.G., Tang, S., Baldini, A., 2009. Tbx1 regulates proliferation and
1043 differentiation of multipotent heart progenitors. Circulation research 105, 842-851.

1044 Choi, C.Y., Lee, Y.M., Kim, Y.H., Park, T., Jeon, B.H., Schulz, R.A., Kim, Y., 1999. The
1045 homeodomain transcription factor NK-4 acts as either a transcriptional activator or
1046 repressor and interacts with the p300 coactivator and the Groucho corepressor. The
1047 Journal of biological chemistry 274, 31543-31552.

1048 Christiaen, L., Davidson, B., Kawashima, T., Powell, W., Nolla, H., Vranizan, K.,
1049 Levine, M., 2008. The transcription/migration interface in heart precursors of Ciona
1050 intestinalis. Science 320, 1349-1352.

1051 Christiaen, L., Wagner, E., Shi, W., Levine, M., 2009a. Electroporation of transgenic
1052 DNAs in the sea squirt Ciona. Cold Spring Harbor protocols 2009, pdb prot5345.

1053 Christiaen, L., Wagner, E., Shi, W., Levine, M., 2009b. Isolation of individual cells
1054 and tissues from electroporated sea squirt (Ciona) embryos by fluorescence-activated cell
1055 sorting (FACS). Cold Spring Harbor protocols 2009, pdb prot5349.

1056 Christiaen, L., Wagner, E., Shi, W., Levine, M., 2009c. Whole-mount in situ
1057 hybridization on sea squirt (Ciona intestinalis) embryos. Cold Spring Harbor protocols
1058 2009, pdb prot5348.

1059 Cinnamon, E., Helman, A., Ben-Haroush Schyr, R., Orian, A., Jimenez, G., Paroush,
1060 Z., 2008. Multiple RTK pathways downregulate Groucho-mediated repression in
1061 Drosophila embryogenesis. Development 135, 829-837.

1062 Cinnamon, E., Paroush, Z., 2008. Context-dependent regulation of Groucho/TLE-
1063 mediated repression. Current opinion in genetics & development 18, 435-440.

1064 Cooley, J., Whitaker, S., Sweeney, S., Fraser, S., Davidson, B., 2011. Cytoskeletal
1065 polarity mediates localized induction of the heart progenitor lineage. Nature cell biology
1066 13, 952-957.

1067 Cota, C.D., Davidson, B., 2015. Mitotic Membrane Turnover Coordinates Differential
1068 Induction of the Heart Progenitor Lineage. Developmental cell 34, 505-519.

1069 Cowley, S., Paterson, H., Kemp, P., Marshall, C.J., 1994. Activation of MAP kinase
1070 kinase is necessary and sufficient for PC12 differentiation and for transformation of NIH
1071 3T3 cells. Cell 77, 841-852.

1072 Dalton, S., 2015. Linking the Cell Cycle to Cell Fate Decisions. Trends in cell biology
1073 25, 592-600.

1074 Davidson, B., 2007. Ciona intestinalis as a model for cardiac development. Seminars
1075 in cell & developmental biology 18, 16-26.

1076 Davidson, B., Levine, M., 2003. Evolutionary origins of the vertebrate heart:
1077 Specification of the cardiac lineage in Ciona intestinalis. Proceedings of the National
1078 Academy of Sciences of the United States of America 100, 11469-11473.

1079 Davidson, B., Shi, W., Beh, J., Christiaen, L., Levine, M., 2006. FGF signaling
1080 delineates the cardiac progenitor field in the simple chordate, Ciona intestinalis. Genes &
1081 development 20, 2728-2738.

1082 Davidson, B., Shi, W., Levine, M., 2005. Uncoupling heart cell specification and
1083 migration in the simple chordate Ciona intestinalis. Development 132, 4811-4818.

1084 Delsuc, F., Brinkmann, H., Chourrout, D., Philippe, H., 2006. Tunicates and not
1085 cephalochordates are the closest living relatives of vertebrates. Nature 439, 965-968.

1086 Diogo, R., Kelly, R.G., Christiaen, L., Levine, M., Ziermann, J.M., Molnar, J.L.,
1087 Noden, D.M., Tzahor, E., 2015. A new heart for a new head in vertebrate
1088 cardiopharyngeal evolution. Nature 520, 466-473.

1089 Dumollard, R., Minc, N., Salez, G., Aicha, S.B., Bekkouche, F., Hebras, C.,
1090 Besnardeau, L., McDougall, A., 2017. The invariant cleavage pattern displayed by
1091 ascidian embryos depends on spindle positioning along the cell's longest axis in the
1092 apical plane and relies on asynchronous cell divisions. eLife 6.

1093 Farley, E.K., Olson, K.M., Zhang, W., Brandt, A.J., Rokhsar, D.S., Levine, M.S., 2015.
1094 Suboptimization of developmental enhancers. Science 350, 325-328.

1095 Farley, E.K., Olson, K.M., Zhang, W., Rokhsar, D.S., Levine, M.S., 2016. Syntax
1096 compensates for poor binding sites to encode tissue specificity of developmental
1097 enhancers. Proceedings of the National Academy of Sciences of the United States of
1098 America 113, 6508-6513.

1099 Gainous, T.B., Wagner, E., Levine, M., 2015. Diverse ETS transcription factors
1100 mediate FGF signaling in the Ciona anterior neural plate. Developmental biology 399,
1101 218-225.

1102 Gandhi, S., Haeussler, M., Razy-Krajka, F., Christiaen, L., Stolfi, A., 2017. Evaluation
1103 and rational design of guide RNAs for efficient CRISPR/Cas9-mediated mutagenesis in
1104 Ciona. Developmental biology 425, 8-20.

1105 George, V., Colombo, S., Targoff, K.L., 2015. An early requirement for nkx2.5 ensures
1106 the first and second heart field ventricular identity and cardiac function into adulthood.
1107 Developmental biology 400, 10-22.

1108 Gopalakrishnan, S., Comai, G., Sambasivan, R., Francou, A., Kelly, R.G., Tajbakhsh,
1109 S., 2015. A Cranial Mesoderm Origin for Esophagus Striated Muscles. Developmental
1110 cell 34, 694-704.

1111 Gotoh, N., Laks, S., Nakashima, M., Lax, I., Schlessinger, J., 2004. FRS2 family
1112 docking proteins with overlapping roles in activation of MAP kinase have distinct
1113 spatial-temporal patterns of expression of their transcripts. FEBS letters 564, 14-18.

1114 Gueroult-Bellone, M., Nitta, K.R., Kari, W., Jacox, E., Beule Dauzat, R., Vincentelli,
1115 R., Diarra, C., Rothbacher, U., Dantec, C., Cambillau, C., Piette, J., Lemaire, P., 2017.
1116 Spacer sequences separating transcription factor binding motifs set enhancer quality and
1117 strength. bioRxiv.

1118 Hasson, P., Egoz, N., Winkler, C., Volohonsky, G., Jia, S., Dinur, T., Volk, T., Courey,
1119 A.J., Paroush, Z., 2005. EGFR signaling attenuates Groucho-dependent repression to
1120 antagonize Notch transcriptional output. Nature genetics 37, 101-105.

1121 Haupaix, N., Abitua, P.B., Sirour, C., Yasuo, H., Levine, M., Hudson, C., 2014. Ephrin-
1122 mediated restriction of ERK1/2 activity delimits the number of pigment cells in the
1123 Ciona CNS. Developmental biology 394, 170-180.

1124 Hotta, K., Mitsuhara, K., Takahashi, H., Inaba, K., Oka, K., Gojobori, T., Ikeo, K.,
1125 2007. A web-based interactive developmental table for the ascidian Ciona intestinalis,
1126 including 3D real-image embryo reconstructions: I. From fertilized egg to hatching larva.
1127 Developmental dynamics : an official publication of the American Association of
1128 Anatomists 236, 1790-1805.

1129 Hu, T., Yamagishi, H., Maeda, J., McAnally, J., Yamagishi, C., Srivastava, D., 2004.
1130 Tbx1 regulates fibroblast growth factors in the anterior heart field through a reinforcing
1131 autoregulatory loop involving forkhead transcription factors. Development 131, 5491-
1132 5502.

1133 Hudson, C., Darras, S., Caillol, D., Yasuo, H., Lemaire, P., 2003. A conserved role for
1134 the MEK signalling pathway in neural tissue specification and posteriorisation in the
1135 invertebrate chordate, the ascidian Ciona intestinalis. Development 130, 147-159.

1136 Hutson, M.R., Zeng, X.L., Kim, A.J., Antoon, E., Harward, S., Kirby, M.L., 2010.
1137 Arterial pole progenitors interpret opposing FGF/BMP signals to proliferate or
1138 differentiate. Development 137, 3001-3011.

1139 Ilagan, R., Abu-Issa, R., Brown, D., Yang, Y.P., Jiao, K., Schwartz, R.J., Klingensmith,
1140 J., Meyers, E.N., 2006. Fgf8 is required for anterior heart field development.
1141 Development 133, 2435-2445.

1142 Imai, K.S., Levine, M., Satoh, N., Satou, Y., 2006. Regulatory blueprint for a chordate
1143 embryo. Science 312, 1183-1187.

1144 Imai, K.S., Satoh, N., Satou, Y., 2002. Early embryonic expression of FGF4/6/9 gene
1145 and its role in the induction of mesenchyme and notochord in Ciona savignyi embryos.
1146 Development 129, 1729-1738.

1147 Jeffery, W.R., Chiba, T., Krajka, F.R., Deyts, C., Satoh, N., Joly, J.S., 2008. Trunk
1148 lateral cells are neural crest-like cells in the ascidian Ciona intestinalis: insights into the
1149 ancestry and evolution of the neural crest. Developmental biology 324, 152-160.

1150 Jerome, L.A., Papaioannou, V.E., 2001. DiGeorge syndrome phenotype in mice
1151 mutant for the T-box gene, Tbx1. Nature genetics 27, 286-291.

1152 Kaplan, N., Razy-Krajka, F., Christiaen, L., 2015. Regulation and evolution of
1153 cardiopharyngeal cell identity and behavior: insights from simple chordates. Current
1154 opinion in genetics & development 32, 119-128.

1155 Kattman, S.J., Witty, A.D., Gagliardi, M., Dubois, N.C., Niapour, M., Hotta, A., Ellis,
1156 J., Keller, G., 2011. Stage-specific optimization of activin/nodal and BMP signaling
1157 promotes cardiac differentiation of mouse and human pluripotent stem cell lines. Cell
1158 stem cell 8, 228-240.

1159 Keduka, E., Kaiho, A., Hamada, M., Watanabe-Takano, H., Takano, K., Ogasawara,
1160 M., Satou, Y., Satoh, N., Endo, T., 2009. M-Ras evolved independently of R-Ras and its
1161 neural function is conserved between mammalian and ascidian, which lacks classical
1162 Ras. Gene 429, 49-58.

1163 Kelly, R.G., Jerome-Majewska, L.A., Papaioannou, V.E., 2004. The del22q11.2
1164 candidate gene Tbx1 regulates branchiomeric myogenesis. Human molecular genetics 13,
1165 2829-2840.

1166 Kelly, R.G., Papaioannou, V.E., 2007. Visualization of outflow tract development in
1167 the absence of Tbx1 using an FgF10 enhancer trap transgene. Developmental dynamics :
1168 an official publication of the American Association of Anatomists 236, 821-828.

1169 Khoueiry, P., Rothbacher, U., Ohtsuka, Y., Daian, F., Frangulian, E., Roure, A.,
1170 Dubchak, I., Lemaire, P., 2010. A cis-regulatory signature in ascidians and flies,
1171 independent of transcription factor binding sites. Current biology : CB 20, 792-802.

1172 Kuwajima, M., Kumano, G., Nishida, H., 2014. Regulation of the number of cell
1173 division rounds by tissue-specific transcription factors and Cdk inhibitor during ascidian
1174 embryogenesis. PloS one 9, e90188.

1175 Lemmon, M.A., Schlessinger, J., 2010. Cell signaling by receptor tyrosine kinases. Cell
1176 141, 1117-1134.

1177 Lescroart, F., Chabab, S., Lin, X., Rulands, S., Paulissen, C., Rodolosse, A., Auer, H.,
1178 Achouri, Y., Dubois, C., Bondue, A., Simons, B.D., Blanpain, C., 2014. Early lineage
1179 restriction in temporally distinct populations of Mesp1 progenitors during mammalian
1180 heart development. Nature cell biology 16, 829-840.

1181 Lescroart, F., Hamou, W., Francou, A., Theveniau-Ruissy, M., Kelly, R.G.,
1182 Buckingham, M., 2015. Clonal analysis reveals a common origin between nonsomite-
1183 derived neck muscles and heart myocardium. Proceedings of the National Academy of
1184 Sciences of the United States of America 112, 1446-1451.

1185 Lescroart, F., Kelly, R.G., Le Garrec, J.F., Nicolas, J.F., Meilhac, S.M., Buckingham,
1186 M., 2010. Clonal analysis reveals common lineage relationships between head muscles
1187 and second heart field derivatives in the mouse embryo. Development 137, 3269-3279.

1188 Lescroart, F., Mohun, T., Meilhac, S.M., Bennett, M., Buckingham, M., 2012. Lineage
1189 tree for the venous pole of the heart: clonal analysis clarifies controversial genealogy
1190 based on genetic tracing. Circulation research 111, 1313-1322.

1191 Mandal, A., Holowiecki, A., Song, Y.C., Waxman, J.S., 2017. Wnt signaling balances
1192 specification of the cardiac and pharyngeal muscle fields. Mechanisms of Development
1193 143, 32-41.

1194 Mansour, S.J., Resing, K.A., Candi, J.M., Hermann, A.S., Gloor, J.W., Herskind, K.R.,
1195 Wartmann, M., Davis, R.J., Ahn, N.G., 1994. Mitogen-activated protein (MAP) kinase
1196 phosphorylation of MAP kinase kinase: determination of phosphorylation sites by mass
1197 spectrometry and site-directed mutagenesis. Journal of biochemistry 116, 304-314.

1198 Marques, S.R., Lee, Y., Poss, K.D., Yelon, D., 2008. Reiterative roles for FGF signaling
1199 in the establishment of size and proportion of the zebrafish heart. Developmental biology
1200 321, 397-406.

1201 Mazzoni, E.O., Mahony, S., Iacovino, M., Morrison, C.A., Mountoufaris, G., Closser,
1202 M., Whyte, W.A., Young, R.A., Kyba, M., Gifford, D.K., Wichterle, H., 2011. Embryonic
1203 stem cell-based mapping of developmental transcriptional programs. Nature methods 8,
1204 1056-1058.

1205 Merscher, S., Funke, B., Epstein, J.A., Heyer, J., Puech, A., Lu, M.M., Xavier, R.J.,
1206 Demay, M.B., Russell, R.G., Factor, S., Tokooya, K., Jore, B.S., Lopez, M., Pandita, R.K.,
1207 Lia, M., Carrion, D., Xu, H., Schorle, H., Kobler, J.B., Scambler, P., Wynshaw-Boris, A.,
1208 Skoultchi, A.I., Morrow, B.E., Kucherlapati, R., 2001. TBX1 is responsible for
1209 cardiovascular defects in velo-cardio-facial/DiGeorge syndrome. Cell 104, 619-629.

1210 Michailovici, I., Eigler, T., Tzahor, E., 2015. Craniofacial Muscle Development.
1211 Current topics in developmental biology 115, 3-30.

1212 Michailovici, I., Harrington, H.A., Azogui, H.H., Yahalom-Ronen, Y., Plotnikov, A.,
1213 Ching, S., Stumpf, M.P., Klein, O.D., Seger, R., Tzahor, E., 2014. Nuclear to cytoplasmic
1214 shuttling of ERK promotes differentiation of muscle stem/progenitor cells. Development
1215 141, 2611-2620.

1216 Mosimann, C., Panakova, D., Werdich, A.A., Musso, G., Burger, A., Lawson, K.L.,
1217 Carr, L.A., Nevis, K.R., Sabeh, M.K., Zhou, Y., Davidson, A.J., DiBiase, A., Burns, C.E.,
1218 Burns, C.G., MacRae, C.A., Zon, L.I., 2015. Chamber identity programs drive early
1219 functional partitioning of the heart. Nature communications 6, 8146.

1220 Nathan, E., Monovich, A., Tirosh-Finkel, L., Harrelson, Z., Rousso, T., Rinon, A.,
1221 Harel, I., Evans, S.M., Tzahor, E., 2008. The contribution of Islet1-expressing splanchnic
1222 mesoderm cells to distinct branchiomeric muscles reveals significant heterogeneity in
1223 head muscle development. Development 135, 647-657.

1224 Nevis, K., Obregon, P., Walsh, C., Guner-Ataman, B., Burns, C.G., Burns, C.E., 2013.
1225 Tbx1 is required for second heart field proliferation in zebrafish. Developmental
1226 dynamics : an official publication of the American Association of Anatomists 242, 550-
1227 559.

1228 Norton, J., Cooley, J., Islam, A.F., Cota, C.D., Davidson, B., 2013. Matrix adhesion
1229 polarizes heart progenitor induction in the invertebrate chordate Ciona intestinalis.
1230 Development 140, 1301-1311.

1231 Park, E.J., Ogden, L.A., Talbot, A., Evans, S., Cai, C.L., Black, B.L., Frank, D.U., Moon,
1232 A.M., 2006. Required, tissue-specific roles for Fgf8 in outflow tract formation and
1233 remodeling. Development 133, 2419-2433.

1234 Park, E.J., Watanabe, Y., Smyth, G., Miyagawa-Tomita, S., Meyers, E., Klingensmith,
1235 J., Camenisch, T., Buckingham, M., Moon, A.M., 2008. An FGF autocrine loop initiated
1236 in second heart field mesoderm regulates morphogenesis at the arterial pole of the heart.
1237 Development 135, 3599-3610.

1238 Patterson, K.I., Brummer, T., O'Brien, P.M., Daly, R.J., 2009. Dual-specificity
1239 phosphatases: critical regulators with diverse cellular targets. The Biochemical journal
1240 418, 475-489.

1241 Pauklin, S., Madrigal, P., Bertero, A., Vallier, L., 2016. Initiation of stem cell
1242 differentiation involves cell cycle-dependent regulation of developmental genes by Cyclin
1243 D. Genes & development 30, 421-433.

1244 Pauklin, S., Vallier, L., 2013. The cell-cycle state of stem cells determines cell fate
1245 propensity. Cell 155, 135-147.

1246 Peljto, M., Wichterle, H., 2011. Programming embryonic stem cells to neuronal
1247 subtypes. Current opinion in neurobiology 21, 43-51.

1248 Pennati, R., Ficetola, G.F., Brunetti, R., Caicci, F., Gasparini, F., Griggio, F., Sato, A.,
1249 Stach, T., Kaul-Strehlow, S., Gissi, C., Manni, L., 2015. Morphological Differences
1250 between Larvae of the Ciona intestinalis Species Complex: Hints for a Valid Taxonomic
1251 Definition of Distinct Species. PloS one 10, e0122879.

1252 Picco, V., Hudson, C., Yasuo, H., 2007. Ephrin-Eph signalling drives the asymmetric
1253 division of notochord/neural precursors in Ciona embryos. Development 134, 1491-1497.

1254 Prall, O.W., Menon, M.K., Solloway, M.J., Watanabe, Y., Zaffran, S., Bajolle, F., Biben,
1255 C., McBride, J.J., Robertson, B.R., Chaulet, H., Stennard, F.A., Wise, N., Schaft, D.,
1256 Wolstein, O., Furtado, M.B., Shiratori, H., Chien, K.R., Hamada, H., Black, B.L., Saga, Y.,
1257 Robertson, E.J., Buckingham, M.E., Harvey, R.P., 2007. An Nkx2-5/Bmp2/Smad1
1258 negative feedback loop controls heart progenitor specification and proliferation. Cell 128,
1259 947-959.

1260 Putnam, N.H., Butts, T., Ferrier, D.E., Furlong, R.F., Hellsten, U., Kawashima, T.,
1261 Robinson-Rechavi, M., Shoguchi, E., Terry, A., Yu, J.K., Benito-Gutierrez, E.L., Dubchak,
1262 I., Garcia-Fernandez, J., Gibson-Brown, J.J., Grigoriev, I.V., Horton, A.C., de Jong, P.J.,
1263 Jurka, J., Kapitonov, V.V., Kohara, Y., Kuroki, Y., Lindquist, E., Lucas, S., Osoegawa, K.,
1264 Pennacchio, L.A., Salamov, A.A., Satou, Y., Sauka-Spengler, T., Schmutz, J., Shin, I.T.,
1265 Toyoda, A., Bronner-Fraser, M., Fujiyama, A., Holland, L.Z., Holland, P.W., Satoh, N.,
1266 Rokhsar, D.S., 2008. The amphioxus genome and the evolution of the chordate
1267 karyotype. Nature 453, 1064-1071.

1268 Racioppi, C., Kamal, A.K., Razy-Krajka, F., Gambardella, G., Zanetti, L., di Bernardo,
1269 D., Sanges, R., Christiaen, L.A., Ristoratore, F., 2014. Fibroblast growth factor signalling
1270 controls nervous system patterning and pigment cell formation in Ciona intestinalis.
1271 Nature communications 5, 4830.

1272 Razy-Krajka, F., Lam, K., Wang, W., Stolfi, A., Joly, M., Bonneau, R., Christiaen, L.,
1273 2014. Collier/OLF/EBF-Dependent Transcriptional Dynamics Control Pharyngeal
1274 Muscle Specification from Primed Cardiopharyngeal Progenitors. Developmental cell 29,
1275 263-276.

1276 Reifers, F., Walsh, E.C., Leger, S., Stainier, D.Y., Brand, M., 2000. Induction and
1277 differentiation of the zebrafish heart requires fibroblast growth factor 8
1278 (fgf8/acerebellar). Development 127, 225-235.

1279 Satou, Y., Imai, K.S., Satoh, N., 2004. The ascidian Mesp gene specifies heart
1280 precursor cells. Development 131, 2533-2541.

1281 Shi, W., Levine, M., 2008. Ephrin signaling establishes asymmetric cell fates in an
1282 endomesoderm lineage of the Ciona embryo. Development 135, 931-940.

1283 Shi, W., Peyrot, S.M., Munro, E., Levine, M., 2009. FGF3 in the floor plate directs
1284 notochord convergent extension in the Ciona tadpole. Development 136, 23-28.

1285 Soufi, A., Dalton, S., 2016. Cycling through developmental decisions: how cell cycle
1286 dynamics control pluripotency, differentiation and reprogramming. Development 143,
1287 4301-4311.

1288 Stolfi, A., Gainous, T.B., Young, J.J., Mori, A., Levine, M., Christiaen, L., 2010. Early
1289 chordate origins of the vertebrate second heart field. Science 329, 565-568.

1290 Stolfi, A., Gandhi, S., Salek, F., Christiaen, L., 2014a. Tissue-specific genome editing
1291 in Ciona embryos by CRISPR/Cas9. Development 141, 4115-4120.

1292 Stolfi, A., Lowe, E.K., Racioppi, C., Ristoratore, F., Brown, C.T., Swalla, B.J.,
1293 Christiaen, L., 2014b. Divergent mechanisms regulate conserved cardiopharyngeal
1294 development and gene expression in distantly related ascidians. eLife 3, e03728.

1295 Stolfi, A., Sasakura, Y., Satou, Y., Christiaen, L., Dantec, C., Endo, T., Naville, M.,
1296 Nishida, H., Swalla, B., Volff, J.-N., Voskoboynik, A., Dauga, D., Lemaire, P., 2014c.
1297 Guidelines for the Nomenclature of Genetic Elements in Tunicate Genomes. Genesis
1298 under review.

1299 Stolfi, A., Wagner, E., Taliaferro, J.M., Chou, S., Levine, M., 2011. Neural tube
1300 patterning by Ephrin, FGF and Notch signaling relays. Development 138, 5429-5439.

1301 Tirosh-Finkel, L., Elhanany, H., Rinon, A., Tzahor, E., 2006. Mesoderm progenitor
1302 cells of common origin contribute to the head musculature and the cardiac outflow tract.
1303 Development 133, 1943-1953.

1304 Tirosh-Finkel, L., Zeisel, A., Brodt-Ivenshitz, M., Shamai, A., Yao, Z., Seger, R.,
1305 Domany, E., Tzahor, E., 2010. BMP-mediated inhibition of FGF signaling promotes
1306 cardiomyocyte differentiation of anterior heart field progenitors. Development 137,
1307 2989-3000.

1308 Tolkin, T., Christiaen, L., 2016. Rewiring of an ancestral Tbx1/10-Ebf-Mrf network for
1309 pharyngeal muscle specification in distinct embryonic lineages. Development in press.

1310 Tzahor, E., 2009. Heart and craniofacial muscle development: a new developmental
1311 theme of distinct myogenic fields. Developmental biology 327, 273-279.

1312 Tzahor, E., Evans, S.M., 2011. Pharyngeal mesoderm development during
1313 embryogenesis: implications for both heart and head myogenesis. Cardiovascular
1314 research 91, 196-202.

1315 Tzahor, E., Kempf, H., Mootoosamy, R.C., Poon, A.C., Abzhanov, A., Tabin, C.J.,
1316 Dietrich, S., Lassar, A.B., 2003. Antagonists of Wnt and BMP signaling promote the
1317 formation of vertebrate head muscle. Genes & development 17, 3087-3099.

1318 Tzahor, E., Lassar, A.B., 2001. Wnt signals from the neural tube block ectopic
1319 cardiogenesis. Genes & development 15, 255-260.

1320 van Wijk, B., van den Berg, G., Abu-Issa, R., Barnett, P., van der Velden, S., Schmidt,
1321 M., Ruijter, J.M., Kirby, M.L., Moorman, A.F., van den Hoff, M.J., 2009. Epicardium
1322 and myocardium separate from a common precursor pool by crosstalk between bone
1323 morphogenetic protein- and fibroblast growth factor-signaling pathways. Circulation
1324 research 105, 431-441.

1325 Vitelli, F., Morishima, M., Taddei, I., Lindsay, E.A., Baldini, A., 2002a. Tbx1 mutation
1326 causes multiple cardiovascular defects and disrupts neural crest and cranial nerve
1327 migratory pathways. Human molecular genetics 11, 915-922.

1328 Vitelli, F., Taddei, I., Morishima, M., Meyers, E.N., Lindsay, E.A., Baldini, A., 2002b.
1329 A genetic link between Tbx1 and fibroblast growth factor signaling. Development 129,
1330 4605-4611.

1331 von Scheven, G., Alvares, L.E., Mootoosamy, R.C., Dietrich, S., 2006. Neural tube
1332 derived signals and Fgf8 act antagonistically to specify eye versus mandibular arch
1333 muscles. Development 133, 2731-2745.

1334 Wagner, E., Stolfi, A., Gi Choi, Y., Levine, M., 2014. Islet is a key determinant of
1335 ascidian palp morphogenesis. Development 141, 3084-3092.

1336 Wang, W., Razy-Krajka, F., Siu, E., Ketcham, A., Christiaen, L., 2013. NK4
1337 antagonizes Tbx1/10 to promote cardiac versus pharyngeal muscle fate in the ascidian
1338 second heart field. PLoS biology 11, e1001725.

1339 Wang, W., Xiang, S., Jullian, E., Kelly, R.G., Satija, R., Christiaen, L., 2017. A single
1340 cell transcriptional roadmap for cardiopharyngeal fate diversification. BioRxiv.

1341 Watanabe, Y., Miyagawa-Tomita, S., Vincent, S.D., Kelly, R.G., Moon, A.M.,
1342 Buckingham, M.E., 2010. Role of mesodermal FGF8 and FGF10 overlaps in the
1343 development of the arterial pole of the heart and pharyngeal arch arteries. Circulation
1344 research 106, 495-503.

1345 Watanabe, Y., Zaffran, S., Kuroiwa, A., Higuchi, H., Ogura, T., Harvey, R.P., Kelly,
1346 R.G., Buckingham, M., 2012. Fibroblast growth factor 10 gene regulation in the second
1347 heart field by Tbx1, Nkx2-5, and Islet1 reveals a genetic switch for down-regulation in the
1348 myocardium. Proceedings of the National Academy of Sciences of the United States of
1349 America 109, 18273-18280.

1350 Whittaker, J.R., 1973. Segregation during ascidian embryogenesis of egg cytoplasmic
1351 information for tissue-specific enzyme development. Proceedings of the National
1352 Academy of Sciences of the United States of America 70, 2096-2100.

1353 Witzel, H.R., Cheedipudi, S., Gao, R., Stainier, D.Y., Dobreva, G.D., 2017. Isl2b
1354 regulates anterior second heart field development in zebrafish. Scientific reports 7,
1355 41043.

1356 Woznica, A., Haeussler, M., Starobinska, E., Jemmett, J., Li, Y., Mount, D., Davidson,
1357 B., 2012. Initial deployment of the cardiogenic gene regulatory network in the basal
1358 chordate, Ciona intestinalis. Developmental biology 368, 127-139.

1359 Yagi, H., Furutani, Y., Hamada, H., Sasaki, T., Asakawa, S., Minoshima, S., Ichida, F.,
1360 Joo, K., Kimura, M., Imamura, S., Kamatani, N., Momma, K., Takao, A., Nakazawa, M.,
1361 Shimizu, N., Matsuoka, R., 2003. Role of TBX1 in human del22q11.2 syndrome. Lancet
1362 362, 1366-1373.

1363 Yasuo, H., Hudson, C., 2007. FGF8/17/18 functions together with FGF9/16/20 during
1364 formation of the notochord in Ciona embryos. Developmental biology 302, 92-103.

1365 Zaffran, S., Frasch, M., 2002. Early signals in cardiac development. Circulation
1366 research 91, 457-469.

1367 Zhang, Z., Huynh, T., Baldini, A., 2006. Mesodermal expression of Tbx1 is necessary
1368 and sufficient for pharyngeal arch and cardiac outflow tract development. Development
1369 133, 3587-3595.
1370